Master's thesis

NTNU
Norwegian University of Science and Technology
Faculty of Engineering
Department of Mechanical and Industrial Engineering

Ranim Hamaied

Wrinkling of Soft Membrane created with Additive Manufacturing: Finite Element Modelling and Analytical validation of existing research

Master's thesis in TMM4960 - Engineering Design and Materials, Master Thesis
Supervisor: Professor Chiara Bertolin
Co-supervisor: Professor Chao Gao
March 2023

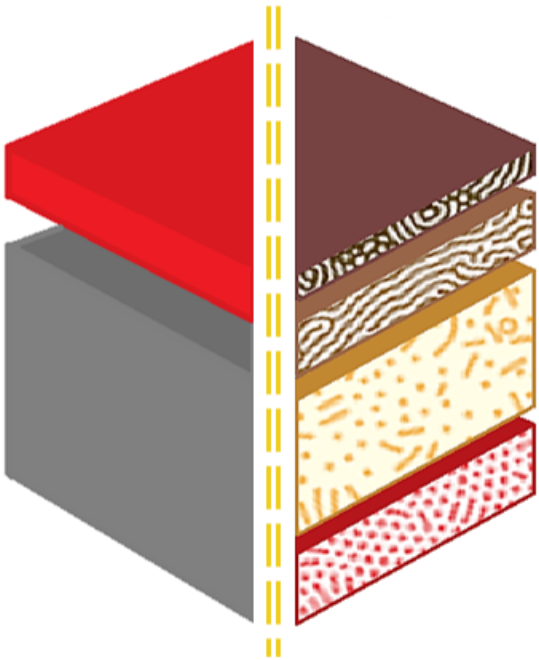

NTNU
Norwegian University of Science and Technology

UNIVERSITÀ DI PARMA

Ranim Hamaied

Wrinkling of Soft Membrane created with Additive Manufacturing: Finite Element Modelling and Analytical validation of existing research

Master's thesis in TMM4960 - Engineering Design and Materials, Master Thesis
Supervisor: Professor Chiara Bertolin
Co-supervisor: Professor Chao Gao
March 2023

Norwegian University of Science and Technology
Faculty of Engineering
Department of Mechanical and Industrial Engineering

NTNU
Norwegian University of
Science and Technology

Abstract

In the leather manufacturing industry, the necessity to introduce new leather-surrogate materials is motivated by the huge environmental footprint of the leather production process. In fact, tanning requires a lot of resources, like water and energy, but also chemicals that can be harmful to the environment and the workers as well. The contribution focuses on how the mechanical characteristics of materials used to imitate leatherlike membranes can be characterised using the wrinkles caused by compressive forces. TPU and PLA, two polymeric materials frequently used in 3D printing based on FDM, are here used to simulate the grain and corium layers of the hide to recreate the skin's structure. A compressive characterization of both materials is performed. In this work, the scientific literature on wrinkling phenomenon has been revised. Wrinkling might form on leather-like soft membranes or in thin layers supported by a substrate when exposed to compressive loading. Results of critical wavelengths determined by the analytical approach using both inputs from experiments and literature, have been finally compared to two combinations of finite element models (FEM) to provide a variety of outcomes and to certify the accuracy of the study. In conclusion, this study provides a preliminary insight regarding the characterization of a 3D-printed, bi-layered material exposed to the wrinkling phenomenon that occurs every day on leather-based products.

Keywords: *Additive Manufacturing; wrinkling; bilayer material; TPU; PLA; soft membrane; leather-like material; sustainability*.

Table of contents

1. INTRODUCTION 1

1.1 The leather industry 2

1.2 State of the Art 6

The wrinkling phenomenon 6

Additive Manufacturing (AM) 7

1.3 Objective 9

1.4 Research questions 10

1.5 Structure of the thesis 10

2 MATERIAL AND METHODS 1

2.1 Material 1

2.1.1 Case of study 1

2.1.2 Raw Material 3

2.2 Methods 5

2.2.1 Printing set up 5

2.2.2 Printing software 8

2.2.3 Compressive Test 9

2.2.4 Critical wavelength calculation by the analytical method 12

Theoretical background 12

Analytical method 15

2.2.5 Critical wavelength evaluated by the numerical simulation 16

3 RESULTS 1

3.1 Printing outcome 1

3.1.1 Compressive specimen outcome 1

3.1.2 Challenges in printing 4

3.1.3 Soft membrane sample with customized Gcode 8

First stage: learning the setting used by SSI slicer 8

Second stage: first interaction with Fullcontrol software 13

Third stage: refinement of the knowledge acquired 17

3.2 Compressive tests outcome 22

3.3 Analytical method outcome 25

3.4 Numerical simulation 27

4 DISCUSSION 1

5 CONCLUSION 1

References 1

1. INTRODUCTION

A common phenomenon that occurs to leather is the wrinkling behaviour that can be triggered by a compressive force. To better understand this problem a large literature exists focusing on surface instabilities of compressed thin film rested on a thick substrate. Such instabilities are widespread in nature. For instance, it can be observed in leaves and flowers [1], but also on human organs like skin, brain, and airways [2-4]. Although, wrinkles are known to be a phenomenon that contributes to the decay of goods new application in the medical and electronical field proves that these instabilities can help to complete several tasks [5].

The knowledge gathered can contribute to a development of the leather industry by substituting the leather with bilayer material that resembles the behaviour and mechanical properties of tanned rawhides to reduce the footprint of this huge industry. The leather structure can be approximated as bilayer system, where the grain and Corium [6], the main layers that define the top grain, are resembled by the film and substrate.

The instability that can occur depends on the nature of the load, compression [7], growth [8], film and substrate mismatching in the mechanical properties [10] and stretching of the substrate [9]. All of these can be the main causes for the formation of wrinkles.

A simple approach to predict the formation of wrinkles and the related wavelength is analysed by the works of Genzer and Groenewold [10] and Cerda and Mahadevan [11] that correlate the mechanical properties of the two materials and the geometry of the membrane with the formation of wrinkles in a bilayer system. In this work, some considerations are made on comparing the analytical method with the studies conducted by Biot [12] that investigated the formation of wrinkles under in-plane compression using the Winkler's foundation theory.

New technologies such as additive manufacturing (AM) which gradually became a popular mean to produce specimens or goods for the industrial production and academic use in the field of soft robotic, biomedical engineering [5] and fashion industry [13] can nowadays

be implemented to speed the production process, reduce the resources employed, and improve the quality control of the finale product.

We present here a bilayer system where the film is composed by Polylactic Acid (PLA) and the substrate with Thermoplastic polyurethane (TPU), both the materials are widely used in AM and present a good bonding. A compressive characterization of the PLA is performed following the ASTM D695 to obtain the values for the compressive strength and Young's Modulus.

In this paper, we will compare the analytical approach presented by Genzer, J, Groenewold [10] with a numerical simulation to validate the theoretical effort toward understanding the wrinkling phenomenon incurred by compressive forces.

1.1 The leather industry

Leather for thousands of years granted a second skin for the humankind providing protection, warmth but also elegance. This precious material was used in several industries and its application is still evolving and changing. As an example, back in the 1960's all ski boots were made of leather (Figure 1.1), but nowadays this kind of product is no longer available [14].

Fig. 1.1. *on the left a leather ski boots, on the right nowadays ski boots.*

This happened in consideration to the new requirements that these boots should reach. In fact, nowadays ski boots must be waterproof, stable, warm, and able to give a good support to the foot shape, and not all these requirements could be achieved using leather as the main material. This replacement was granted by the chemical companies that rapidly developed plastic materials with enviable properties. Despite some industries replaced leather with new advanced materials, the attributes of the hide are still in demand. Durability and strength are a distinctive feature of leather, the same holds for the special appeal leather develops thanks to its craftmanship and uniqueness as product.

The predictions related to the leather industries are based on the present trends, considering the new objectives but also how the industry will satisfy the future demand. To better understand the aim of this work it is important to acquire some knowledge on leather production. Raw material that is been acquired from the meat industry is subject to a series of process known as tanning, a chemical treatment of raw animal hides, to convert it into leather. Tanning agent displaces water from the interstices between the protein fibres and cements these fibres together [15]. The main benefits that hide have after the long-lasting production process are better robustness and strength, resistance to water and heat. The most widely used tanning agent are vegetable and chrome tannin, the first and oldest one seems to have been practiced in prehistoric times [16]. Following the production process for leather the first aspect to take in consideration is raw material. In fact, the balance between natural resources and consumption and population growth must be taken in consideration, as is shown in Figure 1.2.

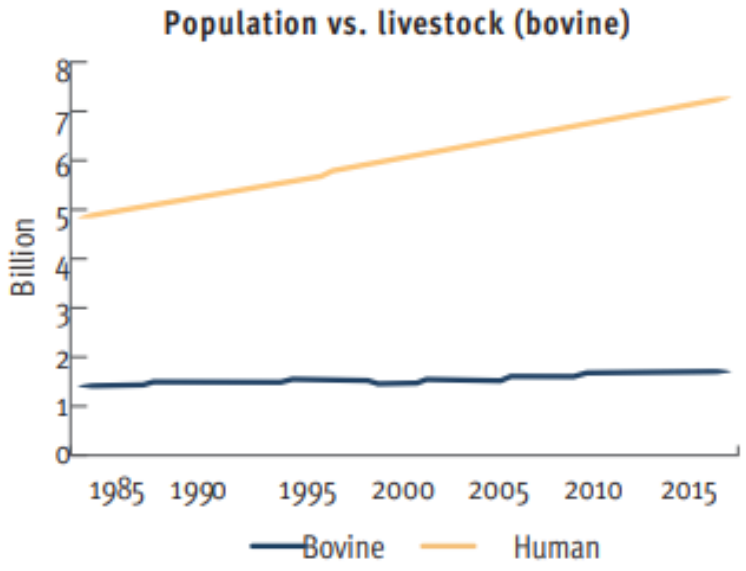

Fig. 1.2. *Annual growth of the human population vs bovine rawhides (reproduced after [17]).*

The growth rate of bovine and ovine raw material base is far behind the growth rate of human population production [17]. This trend can become a problem if in the future there will be a serious food shortage, leading to a choice between hide for leather or for food. It may be that hide utilisation address to the food industry despite the absent of essential amino acids in collagen [14] to contain the food crisis. Therefore, the leather industry will suffer from lack of resources. Moreover, intensive animal farming is one of the many causes known to generate pollution in addition force a low life quality for animal. The second stage of tanning consist of different steps. As an example, here are listed the production steps require for the vegetable tanning process:

1. Curing: the hides are salted to prevent bacteria from growing.
2. Liming: to remove hair and fat residues, the hides are soaked in milk of lime.
3. De-liming: to lower the hides' pH level, they are soaked in another chemical solution.
4. Tanning: over the course of 30-60 days, the hides are regularly moved into different drums filled with tanning solutions of varying concentrations.
5. Drying: the hides are removed from the drums and dried over a few days.
6. Treatment: the leather is oiled, stretched, trimmed, and measured. Depending on how the leather is to be used, other finishing treatments can also be applied.

As it is shown rawhides undergo a long process that uses large amount of natural and chemical resources. Then the energy and carbon footprint and waste management of leather industry remain huge. Environmental regulations in Europe are legislative tools effective in controlling and treating waste that tanneries discharged into the surface waters in the past. Notwithstanding the increasing population still drives a continuous increase in the amount of waste generated to satisfy the leather demand. In the sustainable leather industry, the enhancement of the recyclability and waste reduction can be achieved using more sustainable raw materials and production process management in all the stages of the industrial process (from farm to tanneries to the sale of the finale product).

The scientific community does not have a universally accepted sustainability measuring system and/or unit for the leather industry, but we can find the IPAT described in equation (1.1) gives convincing evaluation of the human impact along with the sustainability approach proposed in the UN Brundtland Commission Report (1987 stating: Sustainability

development is development that meets the needs of the present without compromising the ability of the future generations to meet their own needs) [17].

Human Impact (I) = *Population* (P)**Affluence* (A)**Technology* (T) (0.1)

A represent the consumption per capital while T define the environmental impact per unit of consumption. The key components for a sustainable development range from the environmental aspect to the social aspect taking in consideration the economic factor. This means that a good sustainable production process cannot destabilize the economy of countries or villages that based their development on the leather manufacturing, causing a grow in the unemployed rate that can lead to increase the gap between the rich and poor population. Leather companies struggle to incorporate sustainability due to expensiveness and no short time results. Thus, the alternative it is the introduction of new materials that can be used as a valid alternative to leather to reduce the impact of intensive animal farming and tanneries on the fragile environment. Leather substitutes can offer advantages to the production process, but also it is important to recognize that some substitute material perform better than leather in one or more properties, like described for the ski boots.

The main characteristic required by these new sustainable leather materials should focus on lowering the amount of water consumption, on reducing the chemicals used during the production process, on avoiding hazardous and/or banned substances, and on better controlling quality/re-usability of solid waste, and finally on reducing pollutants reduction such as heavy metal and electrolytes contained therein.

Alternative leather-like materials for fashion leather industry use polyurethane (PU leather), plants and derivates, plant oils or rubber, and fungi, minerals, or living [17]. All those are valid solutions if their carbon footprint is minimized through life cycle assessment (LCA) and Life Cycle Cost (LCC), but a furthermore step can be done by choosing a material that is easiest and quickest to be processed, free from constraints about dimensions, geometry and more. By doing so it is important to achieve a deep knowledge on the material properties and its mechanical behaviour since the stage of the design.

1.2 State of the Art

As described in the previous paragrapher a leather substitute can be a good solution to relief the pressure against the leather industry and thanks to the new advance technology the leather structure can be recreated by new material to achieve better properties. To accurate recreate the leather-like membrane, firstly it is important to understand some of the phenomena that occur daily to tanned rawhides that have an impact on the decay of the material.

The wrinkling phenomenon

This phenomenon can be observed in a wide variety of material and under variegated situation, but it can be easily identified thanks to its unique shape. We can observe wrinkles in our skin, as sign of old age, or on our hands knuckle. In this both cases wrinkles appear as: a consequence of the mechanisms of growth [8] in the underlying layer of the skin for the first example while the formation of wrinkles in the hand's knuckles can be attribute to a compressive force acting on the skin at the moment in which we stretch our fingers. Other ways to trigger this phenomenon can be correlated to the changes in the environmental temperature and humidity [13] these causes a narrowing in the material leading to the formation of wrinkles. Thus, the wrinkles can be described as instabilities that appear as folds and creases due to a wide variety of stimuli that act alone or at the same time.

With this work we will review the scientific aspect of the winging phenomenon as a surface instability that occurs on a bilayer system due to compressive force. Many researches were carried out on this topic and have established that this phenomenon does not only participate to the decay of goods like leather product but it can be useful in several industries [1-5]. Moreover, the extensive research contributes to understand the underlying principles related to the formation of the surface instabilities. Analytical approaches like the one proposed by Biot [12] correlate the wrinkling phenomenon to the Winlker model while the works of Genzer and Groenewold [10], and Cedra and Mahadevan [11] based their assumption on a simple bilayer model that has been used in the past half decade.

These approaches can be used to describe the wrinkling phenomenon in a bilayer system that mimics the leather structure. Therefore, an investigation on the validity of these analytical methods needs to be performed. By doing so a contribution towards the renovation of the leather industry can be made.

Additive Manufacturing (AM)

The outdate tanning technics still used in the tanneries to treat rawhides represent a barrier toward a more sustainable mean of production. Therefore, new techniques can contribute to change the leather industry. The solution proposed by this work is Additive manufacturing (AM), known also as 3D printing, i.e., a technic that builds physical object from a computer-aided design. *The America Society for Testing and Material* (ASTM) define AM as "The process of joining materials to create objects from 3D model data, usually layer by layer, as opposed to fabrication methods by subtraction" [18]. Although this mean of production is slowly spreading in different industries like aerospace industry, automotive industry, medical field it is getting kwon as well in the fashion industry [19]. For instance, the footwear sector that uses leather as raw material introduced additive manufacturing as a mean of production. At the beginning, AM was used for prototypes achieving resounding success by speeding the design validation process, later well-known brands like Nike developed a running shoe model, *Nike FlyPrint*, which production process for the upper part of the shoe was made using AM, furthermore the material used was TPU [20]. Another application is proposed by Mogas-Soldevila et al. [13] that developed some studies using AM as a mean to produce a purse that can be customized based on the pattern dimension, flexibility, opacity, and responsiveness to the temperature. This innovative use of the AM process was possible thanks to the wide range of printing techniques that are available in the market and can be used.

ASTM classified seven AM Technics summarized in Figure 1.3.

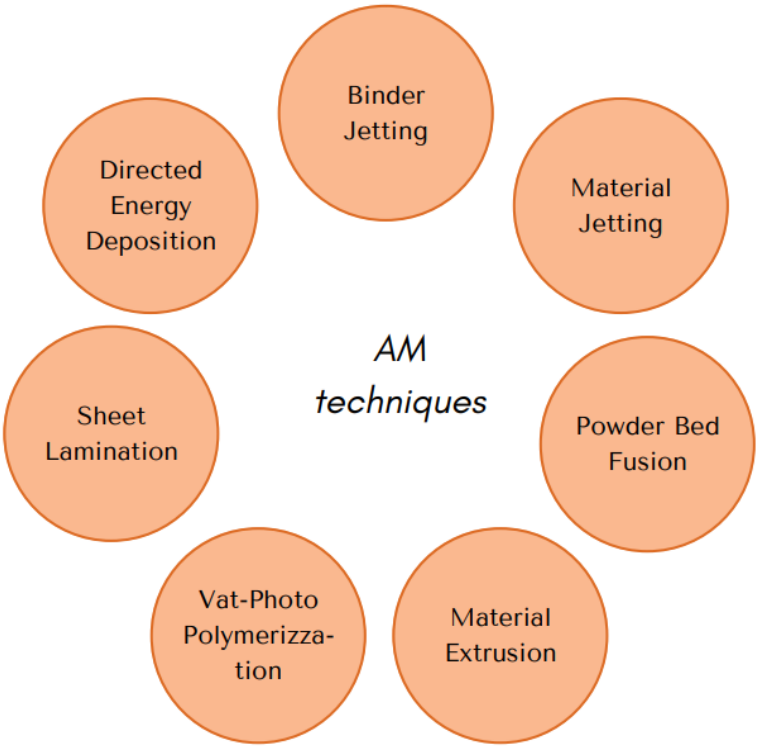

Fig. 1.3. *Classification of the AM techniques based on the ASTM regulation.*

Each of them can be used based on the desire of the user or on the material and required design construction [19]. Types of 3D printing are:

- FDM (Fused Deposition Modelling): the thermoplastic filament spool introduced in the printer is heated up to its melting point (this process happens inside the extruder, i.e., a component of the printing machine) and then get extruded and deposited layer-by-layer base on the 3D solid object designed.
- SLS (Selective Laser Sintering): this type of printing is performed using a laser that tracts the geometry inside a chamber that contains a powder. Later the powder is heated up and get fused together to form a solid object.
- SLA (Stereo-lithography): the liquid resin polymer is cured with UV light, and it gets hardened up instantly.
- LOM (Laminated Object Manufacturing): a supply material like paper, plastic or metal is glued together and later cut using a laser cutter, that removes the areas which are not part of the 3D solid object designed.
- SLD (Selective Deposition Lamination): the machine uses paper and glue. The adhesive nozzle deposits a generous amount of glue in the area that will become part

of the solid while in the surrounding zone the quantity is lower. Latter a piece of paper is added, and the procedure start again. Once the design is finished the paper is cut to eliminate the additional material.

In addition, AM can have a strong impact on the production process. In fact, if we think about the leather industry the production process necessity of several steps that are time-consuming and expensive, with the introduction of AM we can rely on a process that does not need additional processes (i.e., leather splitting, curing, liming) or multiple machines [21].

1.3 Objective

The present thesis is subdivided in two parts. The first part aims to review the scientific knowledge by:

(1) summarizing the existing knowledge related to soft membranes and their behaviour after the application of forces, temperature and/or humidity changes. These stressors factors will enhance the formation of wrinkles within the first layer of the leather (-like) material. After a theoretical introduction on the wrinkle's phenomena, the key parameters regarding the correlation of the wavelength of the wrinkles λ and the mechanical properties of the film and the substrate constituting the leather(-like) materials will be presented. These parameters will be searched in the selected literature reviewed papers.

(2) retrieving information on leather-like materials about their origin, structure, stacking (if there are more than one layer) and used printing pattern for performing experimental and/or numerical analysis.

(3) identifying what have been the specific geometries of the specimens studied in the selected papers. This will be done to detect which specimen can be reproduced to estimate the wavelength of wrinkles by novel experimental tests.

The second part of the thesis aims to:

(4) support the mathematical models retrieved from the literature, through a novel numerical simulation done using the finite element analysis (FEA) using the software Straus7.

Finally (5) conduct novel experimental tests and discuss how the obtained results can be used in leather-like membrane and be compared with FEA. This work can serve as input in modelling new membranes that mimic the behaviour of leather, but it can be also useful for

introducing innovative approaches of study in the leather sector in view of enhancing membranes durability and sustainability. Those research questions are studied within the framework of the European project SIRAMM "Structural Integrity and Reliability of Advanced Material obtained through Additive Manufacturing" project (2020-2023), coordinated by the Polytechnic University of Timisoara (UPT, Romania), with partners the Norwegian University of Science and Technology (NTNU, Norway) and the University of Parma (UNIPR, Italy).

1.4 Research questions

The research questions that we are going to answer with this Thesis are the following:

- Is additive manufacturing a valid mean of production for the leather industry?
- Does AM help to speed up the production process?
- Does AM improve the design process?
- How to recreate a leather-like membrane using additive manufacturing?
- Is wrinkling a phenomenon visible in a membrane made of PLA and TPU?
- Are PLA and TPU valid materials to be used to recreate a leather-like membrane?
- Is the analytical approach to estimate the wavelength of the wrinkling phenomenon in a bilayer system comparable with the numerical simulation results?

1.5 Structure of the thesis

The thesis is structured into five main sections. Chapters: beside the introduction (Chapter 1), the thesis contains the "Materials and Methods" chapter (Chapter 2) that describes accurately the process followed to print and determine the mechanical properties of the materials PLA and TPU. This same chapter presents a brief review of the theoretical background of the wrinkling phenomenon that occur on a bilayer system. This chapter is followed by the "Results" section (Chapter 3) that reports the novel outcome obtained after numerical simulation and experimental activity, then Chapter 4: Discussion highlights the

achievements in comparison with the data acquired from the review of the selected papers, highlighting the point of contacts or the discrepancy as well as the still existing gaps that need to be overcome with future research. Finally, the “conclusions” are presented in Chapter 5.

2 MATERIAL AND METHODS

2.1 Material

2.1.1 Case of study

Leather is a durable and flexible material created by tanning animal rawhides and it can be used for many products. Ensuring that this material can endure an aggressive environment that contributes to its wear and tear is a standard requirement for the leather industry. Therefore, a material that can withstand the natural decay is the key to a valid and sustainable substitute for leather.

Rawhide can be described as soft, collagenous connective tissue. Where collagen is a type of structural protein found in animals, that makes up the structure of the cells and tissue [22]. After the tanning process, the fibrous protein maintains its shape—a three-dimensional fibrous wave—and is known to be the main constituent of the skin. Moreover, the dimensions of those fibres allow for distinction between the leather's layers.

Mammalian skins like those of cattle, sheep, and goats have a similar structure that can be divided into three layers, as reported in Figure 2.1a. The region where the hairs are located is known as grain (A); and just underneath where the hair roots are, Corium (B); and finally, Flesh (C) that is the inner region defining the limit layer of the hide forming a boundary between the skin and the muscle of the animal [6]. As shown in Fig. 2.1b, the fibrous protein collagen changes in dimension and orientation at different levels within the hide. The corium (B) has the largest collagen fibres, while the flesh surface (C) has thinner fibres that run in a horizontal plane. Each region described shows different mechanical properties that make leather a unique material. Therefore, a leather substitute should ideally have the same properties as leather or even better ones.

The tanning process has an additional stage where leather is divided into several thinner layers to obtain sections of the skin that have different qualities. This process is called "leather splitting". The outcome of this production phase led to three layers classified as grain split (or top grain), middle split (if the hide is thick enough), and flesh split. The top grain is considered the more valuable section of the skin. In fact, this layer is composed of a grain that has a compact appearance and thinner collagen fibres, and a part of the corium that is characterised by big fibres.

This contribution will study the wrinkling phenomenon in a soft membrane produced artificially with additive manufacturing. To this end, a simplified model of the top-grain leather split with a two-layer membrane will be adopted. In such a model, the grain is substituted with a thin layer called film and the corium with a thicker layer termed the substrate, as reported on the left side of Figure 1a.

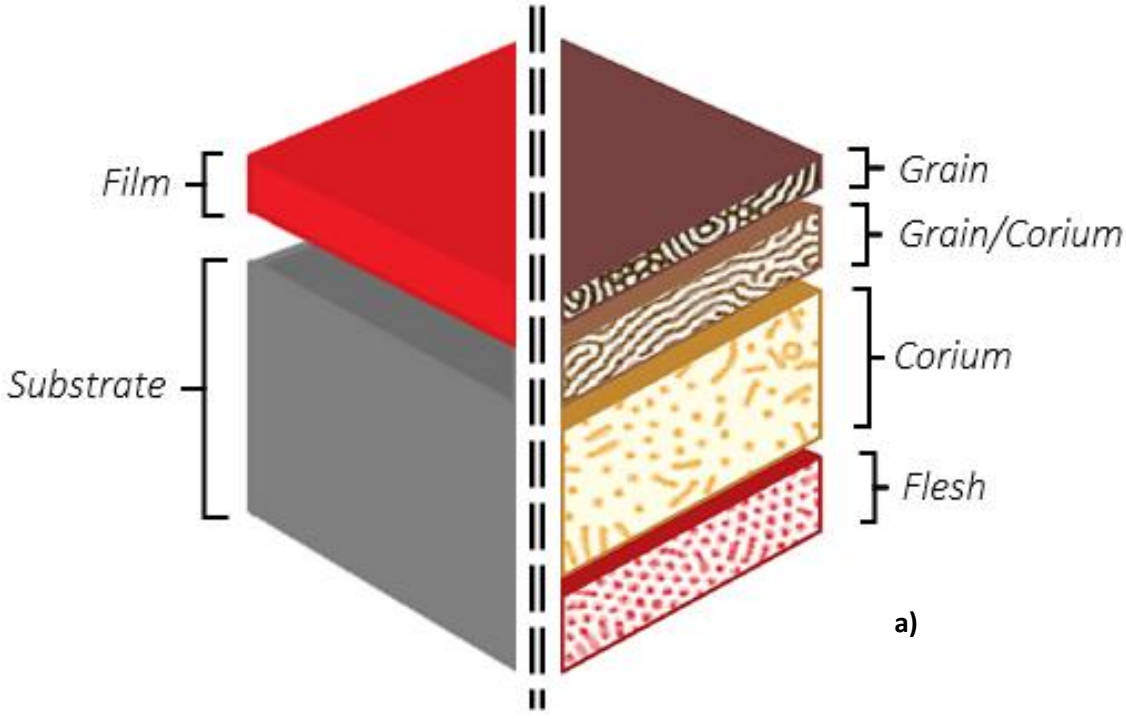

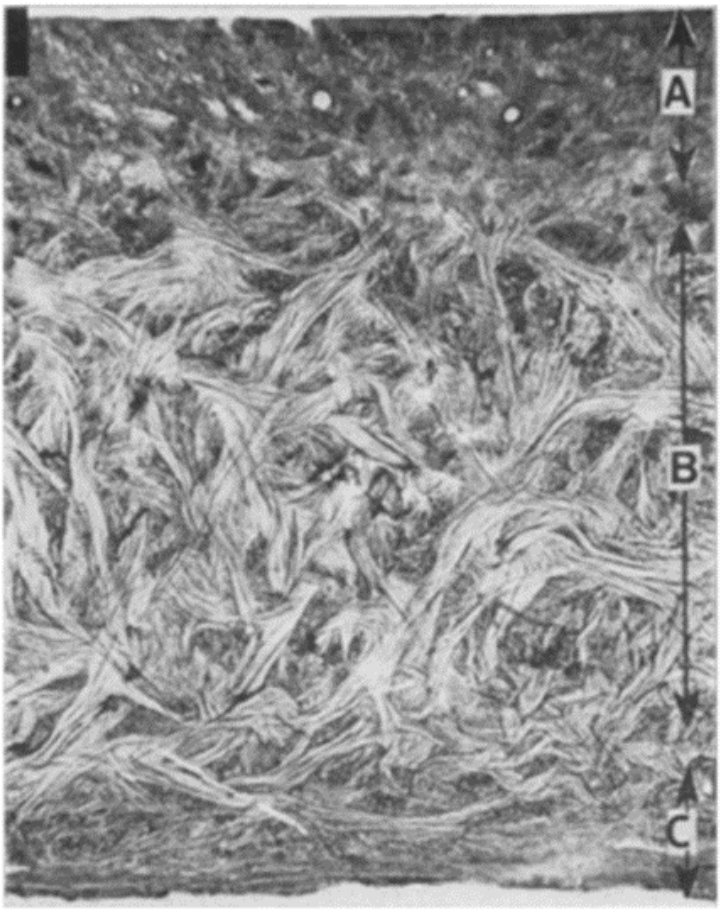

b)

Fig. 2.1. *(a) schematization of the structure of the rawhide and the two-layer system that resembles the top grain; (b) Cross section through cattle skin made into vegetable tanned sole leather, A: grain layer, B: corium, C: flesh layer (reproduced after Haines et al. [6]).*

2.1.2 Raw Material

To choose the more suitable materials for producing a leather-like membrane with good bonding and mechanical properties like or even better than leather, a literature review was carried out. The focus of the search was to learn how, in previous research, the structure of the hide was recreated and tested to evaluate the physical properties of the leather substitute.

In the selection of materials to reproduce leather-like membranes, sustainability played a key role. In fact, in different research conducted in literature a minor footprint means of processing and manufacturing goods within the leather industry were investigated to relive the high environmental impact of this industry [13]. Many works focused on polyurethane (PU) to create an artificial leather polymer made of polyurethane certified to be vegan.

However, the drawback of PU leather is that it does not last due to the cracking and tearing that appear since this material is not flexible like tanned rawhide.

Another solution was presented by Mogas-Soldevila et al. [13] where fashion goods were fabricated with additive manufacturing using leather-like silk protein composites directly derived from Bombyx mori silkworm cocoons, that have been used in the textiles and medical sutures. They combined this material with other chemicals to achieve and enhance some properties. Moreover, materials like TPU have already been used in the footwear industry, this is the case of the design Cevestro that developed an entire shoe using AM as process of production and TPU as main material [20].

Another aspect that was considered during the literature review search was related to the geometries that in the leather-like membranes showed the occurrence of the wrinkling phenomenon. It appeared on a two-layer system comprised of a film bonded to an infinitely deep substrate when the entire membrane underwent compression. The film-substrate module ratio effected the wrinkles [10], as further discussed in the following section.

The materials chosen for reproducing experimentally the bi-layered membrane were selected in order to be compatible with the experimental setup and the analytical models presented in the literature [10].

On these bases, the first selected material was polylactic acid, also known as PLA, an environmentally friendly thermoplastic with a production process that uses less energy than conventional plastic production, thus generating fewer greenhouse gases. In addition, PLA can be easily combined with other materials.

The second selected material for the experiment was the Thermoplastic Polyurethane or TPU, which is widely used in many industries for components, coatings, but also for 3D printing. The production process as for the PLA may be fast and produces small quantity of waste.

2.2 Methods

2.2.1 Printing set up

All the samples were 3D printed by the bi-material printer 3ntr A4V4 (Figure 2.2). An industrial printer with a printing volume of 300x171x200mm. The machine is equipped with three nozzles of 0.3, 0.4, and 0.3 mm. The printer was chosen based on the new applications in the fashion industry [20] and in the research field [13]. In fact, FDM printers guarantee the possibility to use a wide range of materials while at the same time giving the user freedom for dimensions, geometries, and combinations of materials. The diameter of the filament that can be inserted in the machine is 2.85mm for the two first nozzles and 1.75 mm for the third and last nozzle. The nozzle temperature ranges from 90°C to 450°C, and they are equipped with a liquid cooling system. The printing precision is 0.011 mm, and the height of the printed filament ranges from 0.1mm to 0.6mm. Moreover, the chamber of the printer can be heated to print polymers sensitive to the environment temperature. The printing bed is made with carbon material.

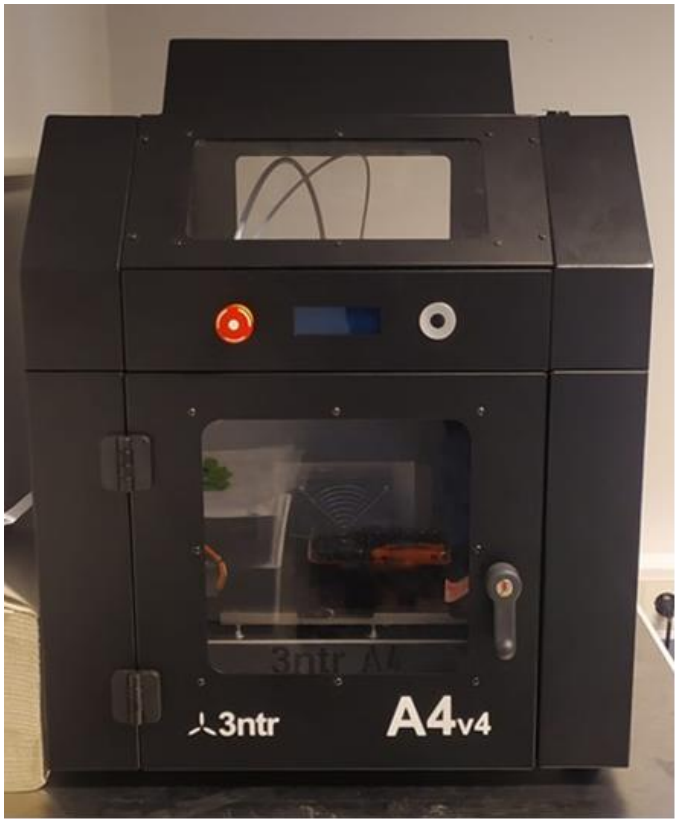

Fig. 2.2. *FDM printer 3ntr A4V4.*

The quality of the produced printed specimens was evaluated based on the filament adherence, the rate of extrusion (to evaluate an over- or under-extruded filament), and the layer's pattern sharpness. PLA specimens were all printed using the first nozzle of 0.3mm and the filament with dimension of 2.85mm (Figure 2.3a). The thickness of the layer was set to 0.15 mm and the temperature, in compliance with the information given by the supplier, ranged from 200° to 210°C. The infill density was set to 100%, and the carbon tray maintained a temperature of 60°C throughout the printing process. In this study, the samples were all printed flat, where both ends of the specimen were in contact with the carbon tray (Figure 2.4).

In order to print TPU specimens, the first 0.3-mm nozzle was adopted, and the filament dimensions were kept similar to those of PLA, e.g., 2.85 mm (Figure 2.3b). Then to guarantee a good bond between the carbon tray and the TPU specimen, the printing process required a second material to be used for the raft (extra extruded material with good bonding properties with the printing bed to fix the specimen throughout the printing process). The printer constructor suggests using PLA or a material known as SSU04. We decided to use PLA to gain more experience on the bonding and printing processes of both PLA and TPU. Therefore, the PLA used for the raft had a filament dimension of 2.85 mm, and the nozzle used had a diameter of 0.4mm. The layer thickness of the TPU specimen was set to 0.15 mm, and the temperature of the nozzle ranged between 220 and 250°C. The infill density was 100% and the bed, since it was in contact only with the PLA raft was set to 60°C that was the set temperature provided by the information given by the supplier. As for the PLA specimens both ends of the printed element were in contact with the carbon tray.

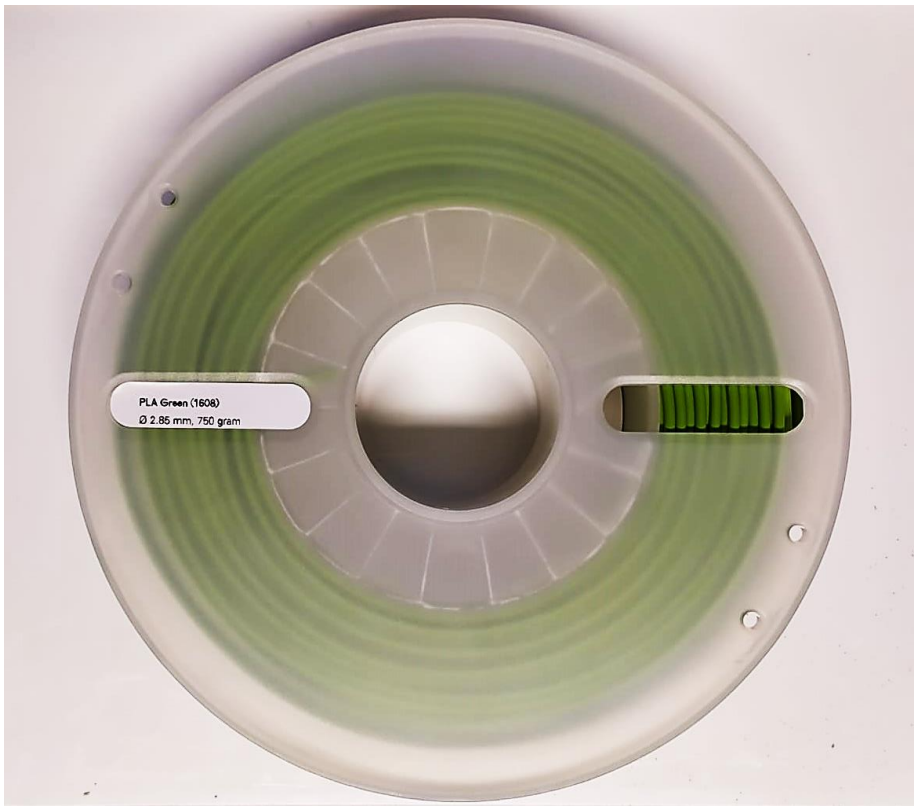

a)

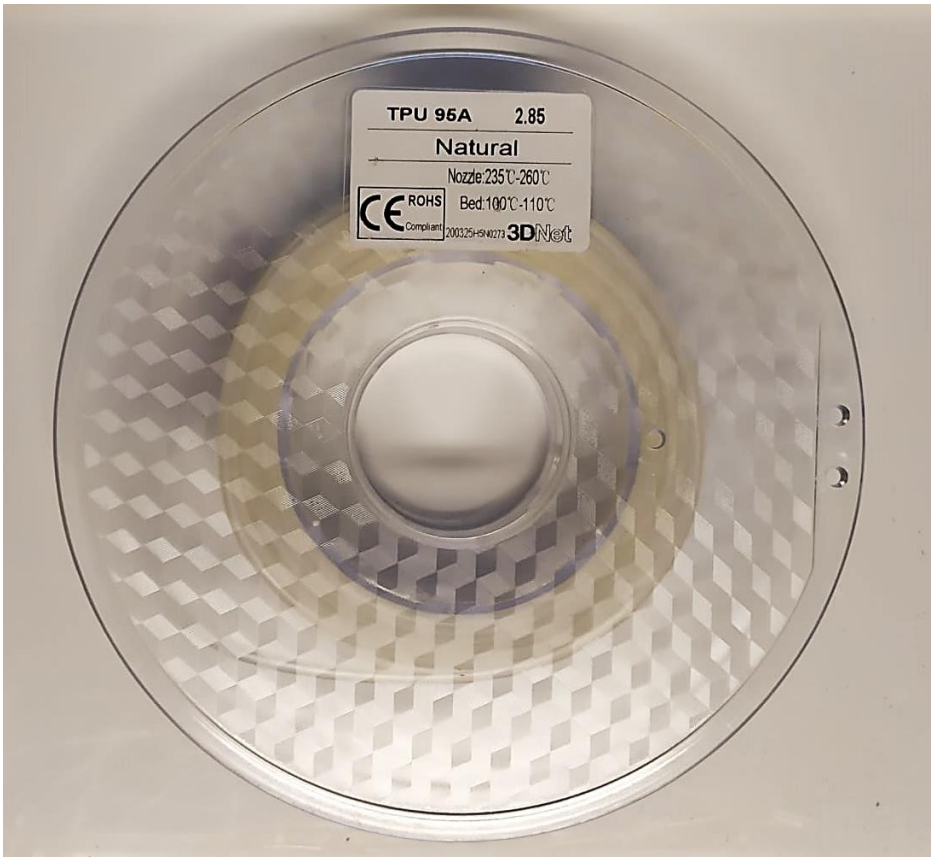

b)

Fig. 2.3. *(a) PLA spool with filament dimeter of 2.85mm; (b) TPU spool with filament dimeter of 2.85mm.*

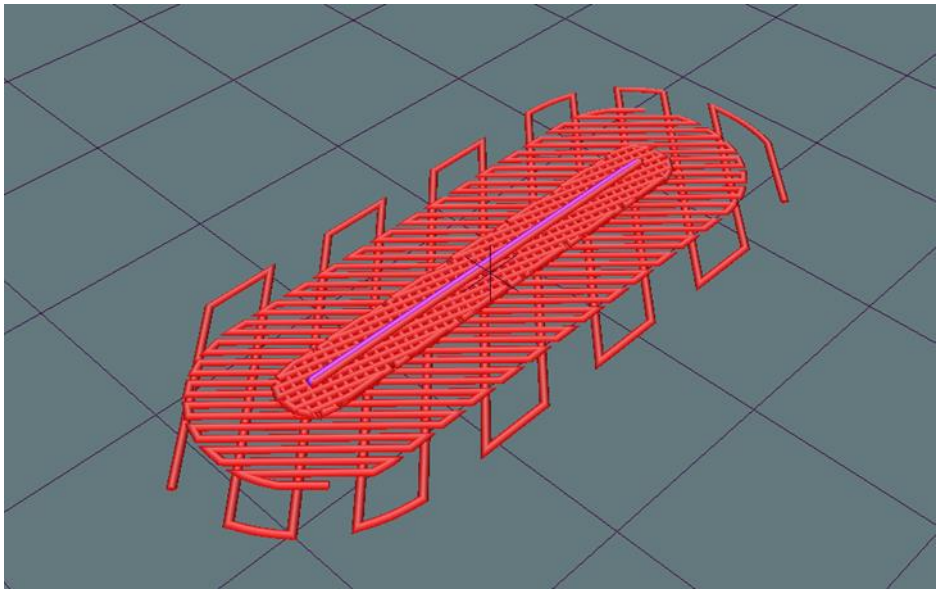

Fig. 2.4. orientation of the printing specimen showed for a simple printing element.

2.2.2 Printing software

The design of the samples was done by SSI and Full Control software. Both of these software programmes were used to achieve a printing design and pattern that could be used for the study on the membrane. The process may be summarized as follows. After the slicing of the model is done, the design of the specimen is converted into a G-Code, which gives instructions to the machine on the coordinates, speed of printing, and extrusion rate for the nozzle to print the model. Once the printing starts, the nozzles heat up to a defined temperature, listed in the G-Code, and begin moving depending on the coordinate, whether it is cartesian or polar. Changing the parameters of the printing process (temperatures, extrusion rate, etc.) can affect the bonding and other aspects related to the mechanical properties, leading to changes in the Young's modulus, peak strength, etc. of the model printed [23].

By using the SSI slicer, the printer introduces an extra piece (called a raft) between the carbon tray and the actual model to assure a good fixture throughout the printing process. Using this technique requires choosing a printing material and a support material that can be constituted by two different materials or simply the same material. During the printing

process, these materials are heated up to the melting temperature, and then they get extruded through the nozzle, which can move according to the coordinates inserted in the G-code. The printing is done by extruding layers on layers, and the cooling happens while the printing is still ongoing, hence once the printing is finished.

2.2.3 Compressive Test

To characterise the compressive mechanical behaviour of the PLA, tests were carried out following the ASTM D695 [24] standard for rigid plastic, to achieve values about the modulus of elasticity (used to define the material in the finite element simulation) and the compressive strength. To prepare the specimen so that the mechanical properties evaluated could be used to describe the behaviour of a bi-layer membrane, the same load condition regarding the filament printing direction was reproduced. In fact, the direction and patterns used in the specimen could lead to a significant difference in the mechanical properties, as highlighted by Yadav et al. [25], who did experimental tests on different specimens printed with several patterns and showed how the infill design and the infill density had an impact on their compressive strength.

The printing pattern and loading condition of the specimens tested in this contribution were printed with a +/- 45° pattern to resemble the leather-like membrane.

The test specimens were designed in compliance with the regulations provided by the standards for test specimen dimensions for strength measurements. As a result, the produced specimens had a prismatic shape with a length twice its principal width (12,7*12,7*25,4 mm3), and the specimen was rotated so that the +/- 45° layers were parallel to the printing plate (Figure 2.5). Five specimens were tested for PLA.

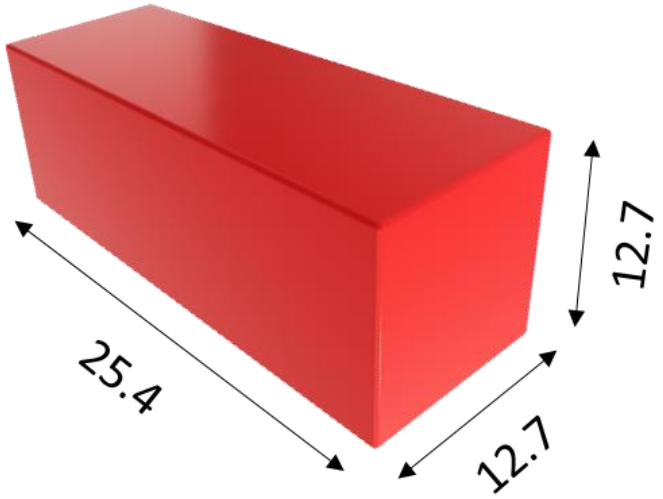

Fig. 2.5. *prismatic specimens used for the compressive test; the dimensions follow the ASTM D695 regulation and are expressed in mm.*

The machine used for the compressive test is an Instron Model 1342 (see Figure 2.6), a servo hydraulic machine with a load capacity of 100kN (the machine is in the NTNU-Norwegian University of Science and Technology Fatigue lab).

To better describe the mechanical properties, five specimens were tested, aligning the principal axis with the load axis, and the speed of testing was set to 1,3 mm per minute (0.050 in per minute). The displacement of the compressive disc attached to the machine was directly obtained from the measurement of the machine. The Young's module was determined considering the linear part of the true stress-strain curve, and the slope was estimated by a linear adjustment. The settings are summarised in Table 2.1.

Table 2.1. *testing settings following the ASTM D695*.

Number of specimens	Rate of displacement	Max displacement set in the machine
5	1.3 mm/min	6 mm

a)

b)

Fig. 2.6. *(a) Instron Model 1342; (b) compressive disk attached to the machine.*

The stress-strain used for the elaboration of the data acquired from the compressive tests, represent the true stress and true strain evaluated using the following expressions.

$$True\ strain = ln(1 - engineering\ strain) \tag{0.2}$$

$$True\ stess = (engineering\ stress) * (1 - engineering\ strain) \tag{0.3}$$

The relationship between the maximum load achieved during the test and the effective cross-section measured prior to the testing was used to calculate the ultimate engineering stress.

2.2.4 Critical wavelength calculation by the analytical method

Theoretical background

Soft materials like those studied in this work can undergo large deformation and they are especially susceptible to surface instabilities that result in the formation of wrinkles.

This happens to a response to a wide range of stimulation like mechanical forces, changes in temperature, in the relative humidity, and in the ph values [1]. For instance, these instabilities can be observed on the mammal skin but also on a compressed rubber [12]. Understanding how these surface instabilities occur can lead to reconsidering the wrinkles as an advantageous phenomenon rather than as a phenomenon that takes part to the decay of goods like leather. The knowledge gathered found application in the biomedical field and in other sectors. On the other hand, wrinkles can be used to evaluate the mechanical properties linked with this surface instability.

To reproduce a simple model of a leather-like membrane, the top grain layer that rests on top of a thick corium layer has a different microstructure and height that consecutively leads to different mechanical properties. Therefore, the mismatching between the elastic properties of the grain and corium and their relative thickness is linked with the formation and physical appearance of wrinkles. A simple model that has been extensively used in literature to describe the mechanical behaviour of a thin film resting on top of a soft elastic foundation [10], has been exploited in this contribution to understand how the wrinkles are formed within the skin. In the model the leather has a film with thickness *h* and width *w* and it is strongly bonded with half-space elastic substrate (see Figure. 2.7). The simplifying hypothesis do not consider the shear stress between the two layers. The mechanical parameters involved are the elastic modulus and the Poisson ratio of the film (E_f, ν_f) and the substate (E_s, ν_s), while the geometrical properties are the thickness of the film and the width of the membrane that for simplification can be taken equal to unity. Plane strain condition is assumed for the bilayer. To trigger the formation of wrinkles a compressive action is applied in the direction reported in Figure 2.7, specifically by applying uniform imposed displacements along the edge. The model can estimate the entity of the resulting force acting on the elastic foundation and describe the wrinkles based on the wavelength λ.

$$F = E_f \left[\left(\frac{\pi}{\lambda} \right)^2 \frac{wh^3}{3\left(1-\nu_f^2\right)} + \left(\frac{\lambda}{\pi} \right) \frac{E_s w}{\pi 4(1-\nu_s^2)E_f} \right] \tag{0.4}$$

λ denotes the wavelength of the surface instabilities of the film along the direction of the applied compressive force that is acting on the substrate. Once the loading is equal or bigger than the critical load F_c surface wrinkling occurs in the film. The corresponding critical wavelength λ_c can be obtained by posing the derivative of equation (1.4) with respect to λ equal to zero. By doing so the critical wavelength is equal to:

$$\lambda_c = 2\pi h \left[\frac{\left(1-\nu_s^2\right)E_f}{3\left(1-\nu_f^2\right)E_s} \right]^{1/3} \tag{0.5}$$

In equation (1.5) the critical wavelength of the wrinkles depends only on the mechanical properties of the material (elastic modulus and Poisson ratio) and on the thickness of the film *h* being independent from the applied stress and strain. It is observed that for small value of *h* and (E_f/E_s) the wrinkling period is very small while it increases if both *h* and (E_f/E_s) increase.

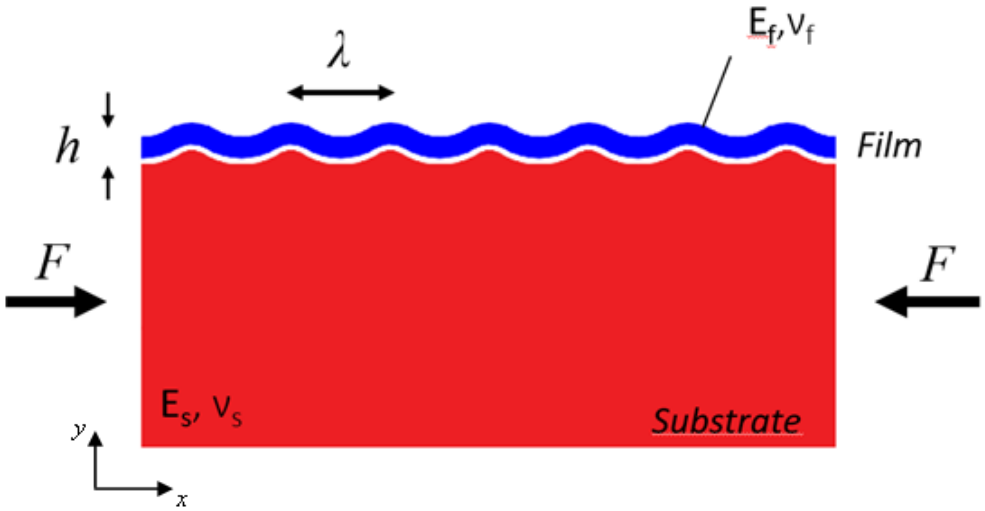

Fig. 2.7. *Sketch of the model adopted for the analytical and numerical resolution*.

Another observation can be made considering a portion of the bilayer with length λ. Assuming a sinusoidal deflection of the surface film with no debonding between the film and the substrate, interface pressures between the two layers develop. Their distribution

along the interface (see eq. 1.6), i.e., with respect to the coordinate *x*, can be determined by considering the analytical solution of a frictionless contact problem available in the literature [26]. In particular, if one takes the frictionless contact problem of a rigid sinusoidal punch pressed against an elastic half-space, the interface pressure turns out to be described by:

$$q(x) = wp(x) = \frac{2\pi E_f^* h_0 w}{\lambda} \cos^2\left(\frac{\pi x}{\lambda}\right) \tag{0.6}$$

$$E_i^* = \frac{E_i}{1-\nu_i^2} \qquad i = s, f \tag{0.7}$$

Where h_0 and w represent the dimension of the cross section of the film and lambda is the wavelength of the wrinkles that appear on the rigid surface. The total potential energy (TPE), V(v), of the system (reported in eq. 1.8) is made up by the contribute of the flexural energy of the skin (E^*_s), the compressive deformation of the substrate, and the work produced by the compressive force F, namely:

$$V(v) = \frac{1}{2}\int_{-\lambda/2}^{\lambda/2}\left(E_s^* I\ddot{v}^2 - F\dot{v}^2 + \frac{q}{h_0}v^2\right)dx \tag{0.8}$$

Supposing that:

$$v(x) = A\cos\left(\frac{\pi x}{\lambda}\right) \tag{0.9}$$

Where A is the amplitude of the wrinkling waves, and the coordinate axis is such that -λ/2≤0≤+λ/2 along x. The TPE can be written as:

$$V_2(v) = \frac{1}{4}A^2\lambda\left[E_s^* I\left(\frac{\pi}{\lambda}\right)^4 - F\left(\frac{\pi}{\lambda}\right)^2 + \frac{3}{2}\frac{\pi}{\lambda}E_f^* w\right] \tag{0.10}$$

The equilibrium is obtained by stationarity condition of equation (1.10), that is by posing the derivative of equation (1.10) with respect to A equals to zero. The solution obtained can be written as follows:

$$F = a\lambda^{-2} + b\lambda \tag{0.11}$$

The expression (1.11) is similar to equation (1.4) proposed by Genzer and Groenewold [10] and it resembles the analysis on wrinkles made by Biot in 1962 [12].

Analytical method

To investigate the formation of wrinkles in a two-layer system described in Figure 2.7, the approach introduced in the work of Genzer and Groenewold [10], described by the equations (1.4) and (1.5), was used in this thesis. The analytical analysis was performed on two different membranes. The materials adopted for the two study cases are the same, i.e., PLA used for the thin film that resembles the grain, and TPU employed for the substrate, which is the thicker layer that represents the Corium. The thickness of the film layer was changed to observe the quality of prediction of the wavelength given by the expression (1.5) adopted to estimate the critical wavelength. In the first considered case, the film had a thickness of 1 mm, while in the second case, the thickness was of 0.2 mm.

The hypothesis of the analytical model defines the substate as having an infinite thickness. Therefore, for this evaluation, the substrate does not have a finite thickness. Last, the length of the membrane was chosen after a preliminary evaluation of the critical wavelength. This was possible since the equation (1.5) is not dependent on the length of the bilayer system; to have a better visualisation of the sinusoidal surface instability that forms along the direction of application of the compressive forces, a length of 40 mm was adopted for both case analyses.

As seen in the preview chapters, the analytical approach, in particular, the equation (1.4), depends on the mechanical properties of the two materials (Young’s modulus and Poisson coefficient) and on the thickness of the film. Therefore, the compressive test outcome has been used to estimate the critical wavelength to give better quality results since the mechanical properties obtained from the literature can be evaluated on specimens with different printing patterns and orientations [19; 27–29]. A further commentary is given in the results section of this thesis.

2.2.5 Critical wavelength evaluated by the numerical simulation

A comparison between the analytical results and the numerical analysis was done to validate the analytical method that was used. The numerical simulation analysis was performed using the software Strauss 7. There was the need of conductig some evaluations because the substate in the analytical model had the hypothesis of an infinite thickness. To reproduce this condition, we decided to set the thickness of the substrate to a value that could reduce the elaboration time (for the numerical simulation) while limiting the influence of the finite substrate. To achieve this state, a ratio between the thickness of the skin and the thickness of the substrate was set, respectively, to 1/10 and 1/50 for the two cases analysed (Figure 2.8).

a)

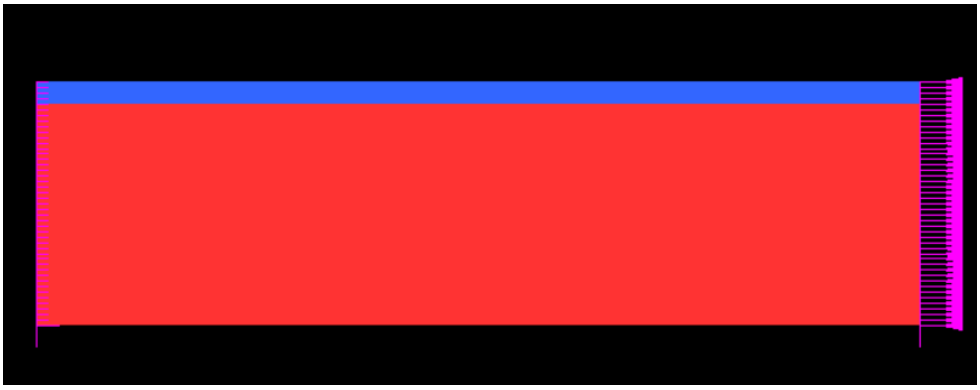

b)

Fig. 2.8. *Representation of the bilayer model used for the analytical and numerical simulation: (a) model with film's thickness of 0.2 mm and substrate thickness of 10 mm, the length is equal to 40 mm; (b) model with film's thickness of 1 mm and substrate's thickness of 10 mm, the length is equal to 40 mm.*

The two-layer, i.e., film and substrate, are modelled as two distinguishable elements plate. For each element, the mechanical properties used are the ones obtained from the compressive tests. Therefore, as shown in Figure 2.9, the Young's module that will be introduced in the FEA corresponds to the average value elaborated from the true stress-strain curve for the five specimens. The mesh used for the model was accurately chosen to obtain the most accurate results. The film along the dimensions of 1 mm and 0.2 mm is described by two elements per plate, while for the substrate, the number of elements are 20. Along the length of the membrane (40 mm for both cases analysed), the number of elements used on the plate is 80. Figure 2.10 shows the mesh used.

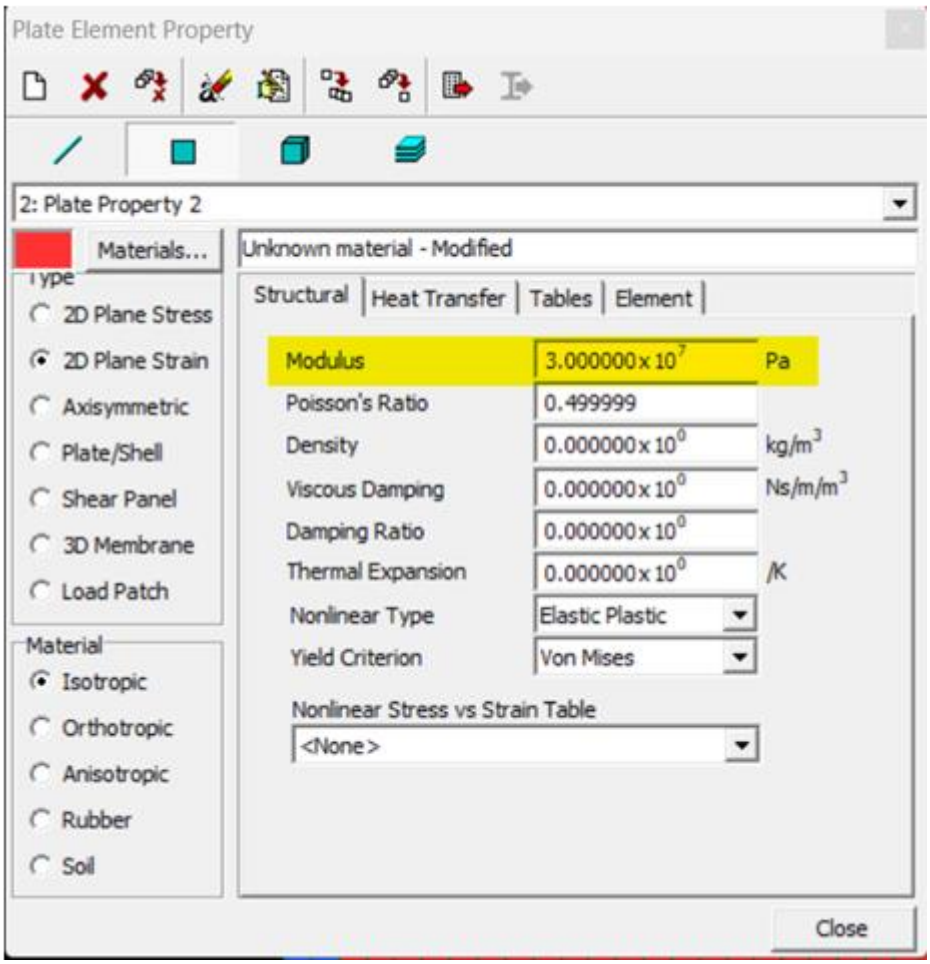

Fig. 2.9. *Representation of the section where the mechanical properties of the material have to be introduced.*

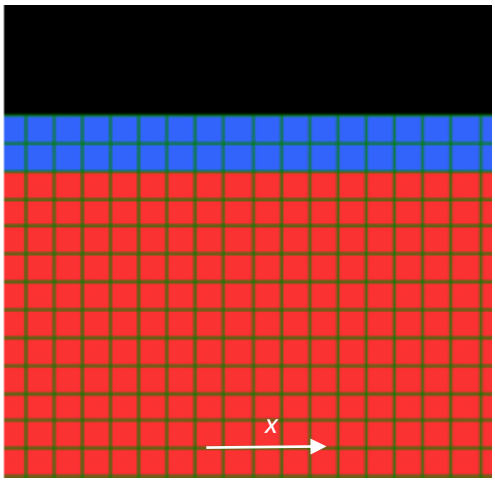

Fig. 2.10. *Representation of the mesh used for the membrane with 0.2 mm film thickness.*

A plain-strain condition was assumed for the membrane. Therefore, to recreate uniform compressive stress on the bilayer system, a displacement of 1 mm was applied to one end of the membrane while the other end was restrained. The analyses that were performed on the model are the linear analysis, the bulking analysis, and the non-linear analysis.

3 RESULTS

3.1 Printing outcome

3.1.1 Compressive specimen outcome

The design of the five specimens required by the ASTM D695 regulation for the compressive tests was made entirely using the SSI software. This is the reason why the designed specimens, as shown in Figure 3.1, have an extra volume of extruded material, a raft, attached to the bottom of the prismatic shape.

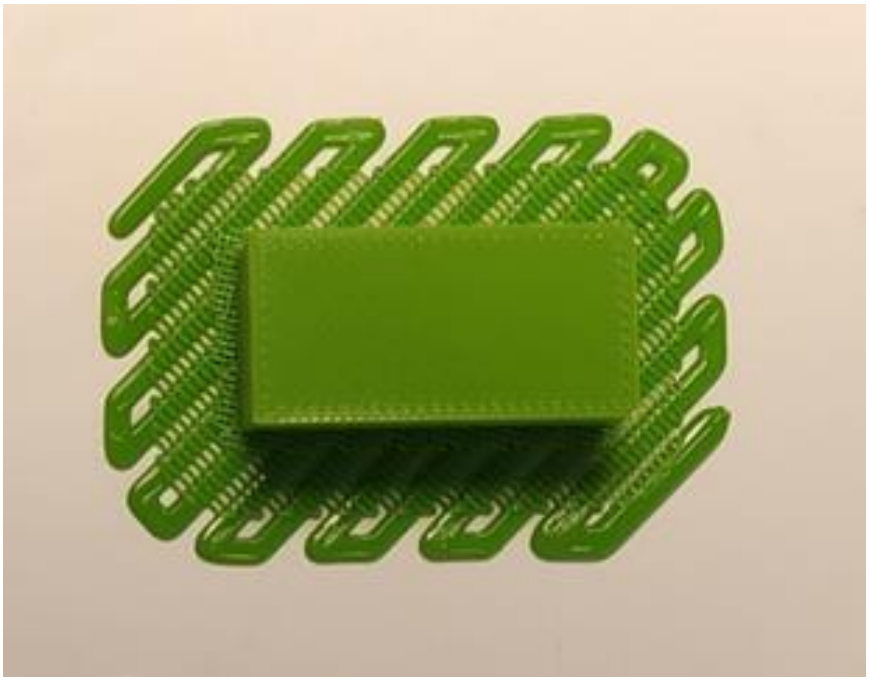

a)

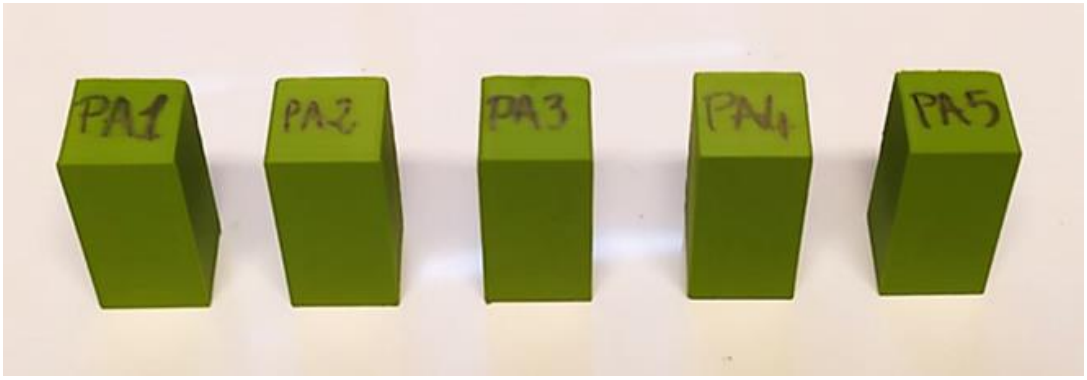

b)

Fig. 3.1. *(a) specimen still attached to the raft; (b) the five specimens used for the compressive test.*

To distinguish the specimens throughout the printing and testing process, a codification was required to correlate the printing date and testing data with the specimen being analysed. The alphanumeric code defines the material used, the load axis for the compressive test, and the printing order. For instance, the specimen's code PA1, i.e., the first specimen in Figure 3.1, is defined with P being the material PLA and with A being the load axis aligned with the longest side (25.4 mm), and the last 1 stating that the specimens were the first to be printed.

The results of the quality printing outcome based on the filament's adherence, extrusion rate, and pattern sharpness as performed only on the prismatic printed shape are listed in Table 3.1.

Table 3.1. *Quality check analysis for the specimens.*

Specimen	Filament's adherence	Over/Under extrusion	Pattern sharpness
PA1	Good	Good	Good
PA2	Good	Good	Good
PA3	Good	Good	Good
PA4	Good	Good	Good
PA3	Good	Good	Good

All the specimens have successfully passed the quality check. In fact, there are no filaments that easily detach from the main body; even after the compression test, good bonding can be observed on the distorted specimens. The extrusion rate was controlled throughout the printing process, and there was no noticeable change in the volume of material extruded. At the same time, the pattern sharpness was evaluated during and after the printing process. The definition of the pattern is clear, as can be seen in Figure 3.1a, where an outer border made of two filaments and a +/-45° filling pattern was visible. A further evaluation was made on the surface of the prismatic specimen that was in contact with the raft. We observed that within this first layer in all the specimens, the infill density was less than 100% (Figure 3.2a).

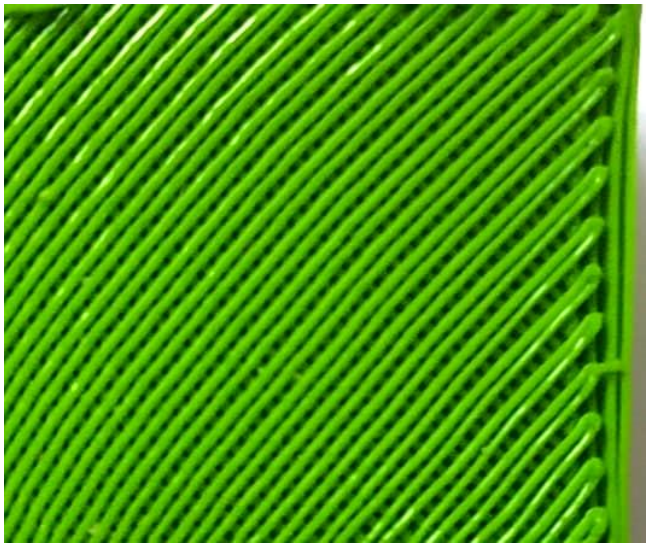

a)

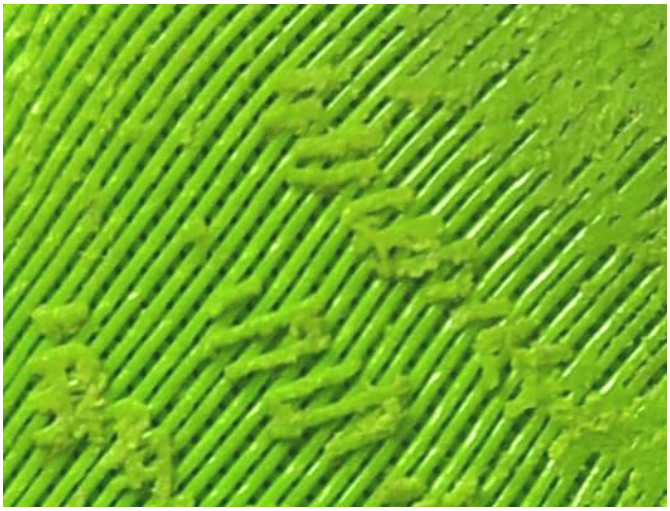

b)

Fig. 3.2. *(a) surface in contact with raft [specimen PA1]; (b) surface in contact with raft [extra specimen introduced to analyze the initial infill density].*

To better investigate if the assigned infill density was reached after a few layers or more, an extra specimen was printed. The process was suddenly interrupted about mid-print to observe if the last layer reached the desired infill density. Since this printing test did not highlight any changes in the infill density with the last printed layers (see Figure 3.2b), we assumed that the first layer is the only one that may show this problem while the infill density of 100% is reached within the other layers.

The analysis of TPU was not possible due to time constraints and printer issues, but more research can be done to resolve the TPU research question. Therefore, in the following section, there is no reference to the TPU.

3.1.2 Challenges in printing

The A4V4 printer was also employed to investigate the G-code and the limits of additive manufacturing. Therefore, a study was conducted on recreating patterns that can be used to print the leather-like membrane. With the knowledge gathered throughout the compressive specimens' printing process, it was clear that the industrial printer and the software outlined some limits. In particular, the SSI software does not contemplate a wide variety of patterns. The user cannot substitute or eliminate the outer filaments that cover the perimeter of the specimen with another pattern, but it is possible to choose the number of filaments from a minimum of two. Another limitation was given for the choice of the infill pattern. The compressive specimens were printed with the software-assigned pattern of +/-45°.

To avoid the limitations given by the SSI software, Gcode had to be written from scratch. It is a complex and time-wasting process that can be avoided using Full Control, a software that helps with the design of the printing models and gives the user the freedom to choose all the aspects of the printing process for every filament extruded, like the direction, speed, extrusion rate, acceleration, temperature of the nozzles, temperature of the bed, and more. By using this software, it is no longer necessary to write the Gcode from scratch; in fact, only the start and end Gcode must be inserted in a specific section of the programme to use the right setting of the FDM printer A4V4. Figure 3.3 shows the start Gcode and end Gcode.

Line 1	;GCode generated with FullContı
Line 2	
Line 3	M75
Line 4	M11
Line 5	M107 ;start with the fan off
Line 6	G91
Line 7	G1 Z1; move z up little to preven
Line 8	G90 ;absolute positioning
Line 9	M190 S60
Line 10	M104 T3 S 210
Line 11	M218 T0 Z-0
Line 12	M218 T1 Z-0
Line 13	M218 T2 Z-0
Line 14	T0
Line 15	G28 Y0
Line 16	G92 Y0
Line 17	G28 X0
Line 18	G28 Z0
Line 19	G1 Z2
Line 20	G92 E0
Line 21	M400
Line 22	G92 E0
Line 23	M400
Line 24	T0
Line 25	M104 S210
Line 26	
Line 27	M109 S210
Line 28	G92 E0
Line 29	M82 ;absolute extrusion mode
Line 30	
Line 31	G92 E0
Line 32	G92 E0
Line 33	
Line 34	M83 ;relative extrusion mode
Line 35	
Line 36	M106 S0 ; set fan speed
Line 37	
Line 38	G0 F4320 X20.0 Y10.0 Z0.3
Line 39	G1 E4 F2700
Line 40	
Line 41	
Line 42	;END OF THE START GCODE

Line 43	;START OF THE END GCODE
Line 44	
Line 45	G1 E-5 F2700
Line 46	
Line 47	M104 S0
Line 48	G92 E0
Line 49	G1 E-8 F1200
Line 50	G92 E0
Line 51	M400
Line 52	M107
Line 53	G92 E0
Line 54	M12
Line 55	M77
Line 56	M107
Line 57	M104 T3 S0
Line 58	M104 T2 S0
Line 59	M104 T1 S0
Line 60	M104 T0 S0
Line 61	M140 S0
Line 62	G1 X10 Y50 F9000
Line 63	G28 X0 Y0
Line 64	M84
Line 65	
Line 66	; 5353492056657273696F6E
Line 67	
Line 68	
Line 69	
Line 70	
Line 71	
Line 72	
Line 73	; END OF END CODE

Fig. 3.3. *at the left the Start Gcode at the right the End Gcode.*

The first three lines of the start Gcode give instructions to the printer regarding auxiliary commands like starting the printing job timer and turning on the internal fan. After, the commands G1 Z1 (Line 7) indicate a movement of the bed to prevent the scratching of the surface by the nozzle (within the Gcode vocabulary, G is used to control what kind of movement the nozzle or bed should do). The temperature of the nozzles used is given by the string "M104 T3 S210" (Line 10) where the value after the letter T points to the nozzle's number and the value after the letter S sets the temperature desired, while the temperature for the carbon tray is described by the string "M109 S60" (Line 9) whereas for the nozzle, the value written after S is referring to the temperature. If there aren't any similar strings in the rest of the Gcode, then the temperature set previously will last till the end of the printing.

Another relevant command introduced in the start Gcode file regards the extrusion mode. In fact, printers can operate using either relative extrusion mode or absolute extrusion mode, which define how to indicate the extruded volume for each command, i.e., string. The first mode will require inserting on each string the volume of the filament, while with the second mode, the extruded volume is equal to the volume of the filament plus the volume printed at the beginning of the printing process. After confronting the SSI Gcode, we observed that the machine could support both printing modes, but FullControl used relative extrusion mode. Therefore, an additional string in the start Gcode was added to define the printing mode, M83.

Nowadays a wide variety of materials used for FMD printing require custom-made settings, like the temperature of the bed or nozzle. For instance, the temperature required at the nozzle to print PLA is different from the temperature used for TPU. Moreover, the chamber temperature can influence the final results during the printing process. Some printers, like the one used for this work, are equipped with a fan that regulates the chamber temperature. Therefore, specific commands need to be added to the start Gcode (or when the material will be printed). The string "M106 S0" (Line 36) allows to turn the fan on and set the speed and temperature of the chamber. Not only the chamber temperature but also the humidity can influence the final product. Since the printer used does not have a device that can control the humidity before, during, and after the printing process, an external dehumidifier can be used to control the room humidity.

The sting "G0 F4320 X20.0 Y10.0 Z0.3" (Line 38) starts with the letter G, which means that the command gives instructions for movement of the nozzle or bed (the A4V4's nozzle can only move in the plane x-y, while the bed can move along z). The starting coordinates for the nozzle are X + 20 mm and Y + 10 mm; the bed will be lowered to 0.3 mm in order to

do not scratch the surface of the tray while the nozzle moves. In this string there is another command related to the speed of the nozzle's movement. In fact, this parameter can be controlled during printing. The value of the letter F gives the velocity of the movement. For instance, if the nozzle is extruding any material and needs to move from the start point to the first point printed, the velocity can be fast, while if the nozzle is extruding a material that requires a more delicate and precise process, a lower velocity can be set. The velocity of the nozzle has a great impact on how long the printing process will last and on the quality of the printed specimen. In fact, a high velocity can influence the bonding between the carbon tray and the extruded filament.

The last command written at the start Gcode introduced another parameter that controls the volume of extruded material. Since the start Gcode does not include any printing filament, but its aim is to prepare the machine to start printing the value after the letter E is set to fill the volume inside the nozzle so that the printing can start immediately to extrude the material for the specimen.

After the sample is printed it is necessary the introduction of an ending Gcode in order to turn off correctly the machine. In Figure 3.3, the end Gcode introduced in the Fullcontrol programme is proposed. The main commands that are listed in this part of the Gcode are those linked to the extrusion rate. In fact, once the printing is over, to prevent the material from dripping and cooling down inside the nozzle, a retraction of the material is performed. The string "G1 E-5 F2700" (Line 45) gives instructions to the machine to retract the material. Other commands relate to the nozzle temperature that can be lowered. The same is applied to the printing bed. To prevent the nozzle from touching the specimen printed and damaging it in the end Gcode, once the printing process is finished, the nozzle will not go back to the start coordinates described in the start Gcode, but it will stay in the same position reached at the end of the printing. To remove the carbon tray, the user should control the movement of both the nozzles and printing bed from the machine display, which gives the possibility to lower the bed with a range of motion from mm to cm at the same time the nozzle can be moved.

The main body of the Gcode that gives the machine the commands to print the specimen is analysed in the following paragraph.

3.1.3 Soft membrane sample with customized Gcode

This paragraph includes a detailed description of the testing that were made to recreate the membrane, describing the steps followed, the outcome and suggestion that were deduced from the gathered knowledge. The analysis will be divided into three subparagraphs:

- First stage: learning the settings used by the SSI slicer
- Second stage: first interaction with Fullcontrol software
- Third stage: refinement of the knowledge acquired

First stage: learning the setting used by SSI slicer

Although a good amount of knowledge was acquired with the printing process of the compressive specimens, the approach that was followed started with an analysis of the basic aspects of the printing. Therefore, simple samples were designed and introduced in the SSI software.

The material used is PLA, since its characteristics allow for an easier printing approach. For instance, the raft introduced by the SSI software can be made using PLA thanks to its good bonding with the carbon tray. For this reason, it represents a good option for printing the specimen with FullControl, on account of the fact that one of the reasons we use this software was to eliminate the raft that could damage the specimen once it has been detached from the main body. In Figure 3.4, it is visible that some filaments of the raft used for the compressive specimens are still attached to the main body. Although this does not influence the results of the compressive test, it can pose a problem for testing on soft membranes that have a thin film made with PLA.

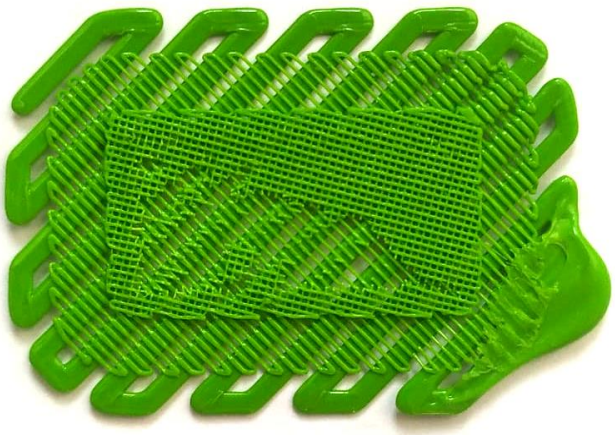

Fig. 3.4. *filaments detached from the raft used for the compressive specimen.*

The temperatures of the nozzle and bed are the same as those adopted for the compressive specimen printing process, i.e., nozzle temperature set between 200–210 °C and bed temperature set at 60 °C.

The SSI slicer automatically generated the Gcode for all the samples printed in this preliminary stage of the study, whose design was made in SOLIDWORKS.

The first printing test was conducted to observe if the quality of the printing is influenced by the printing orientation. The printed specimen is long 20 mm, 10 mm wide, and 1 mm high. Figure 3.5.

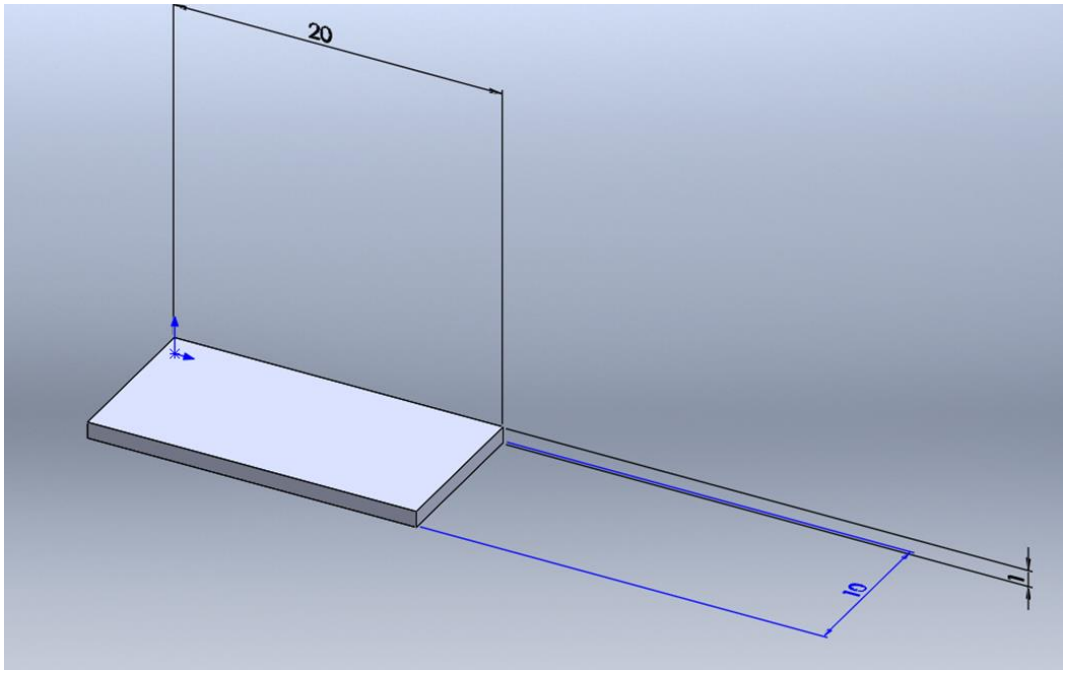

Fig. 3.5. *dimension of the specimen used for the analysis on the printing quality in regard the orientation.*

In this phase, the filament dimensions are not considered. As for the compressive specimens, the infill pattern is +/-45° while the infill density is set to 100%.

The printing orientation evaluated are:

- 0° angle (the long side of the specimen is parallel to the x coordinate given in the SSI software)
- 90° angle (the long side is perpendicular to the x axis of the SSI software)
- 45° angle (the long side is rotated by 45° with regard to the x axis of the SSI software)

All three specimens do not have any noticeable flaws in the printing quality (Figure 3.6). The first specimen (0° angled specimen) shows an over-extrusion of PLA at the beginning of the printing process. This flaw in the extrusion rate is located within the raft, and it happened only for the first specimen. We can suppose that since the printer was not used before, over-extrusion can be avoided by purging the material prior to printing.

Fig. 3.6. *on top the specimen printed with an angle of 0°; on the center the specimen printed with an angle of 90°, at the bottom the specimen printed with an angle of 45°. The specimen outlines some damage that is not related to the printing process.*

The second analysis was made to evaluate and understand the Gcode. Since the infill pattern that we wanted to achieve using Fullcontrol is unidirectional, i.e., all the filaments are aligned, we decided to print two filaments. To achieve the pattern in the SSI software, a sample measuring 24.5 mm long, 0.3 mm wide, and 0.3 mm high was designed in the SOLIDWORKS software and then introduced in the SSI software. Thanks to the small dimension of this specimen, the SSI slicer generated a Gcode where the sample is made of two unidirectional filaments (Figure 3.7a).

a)

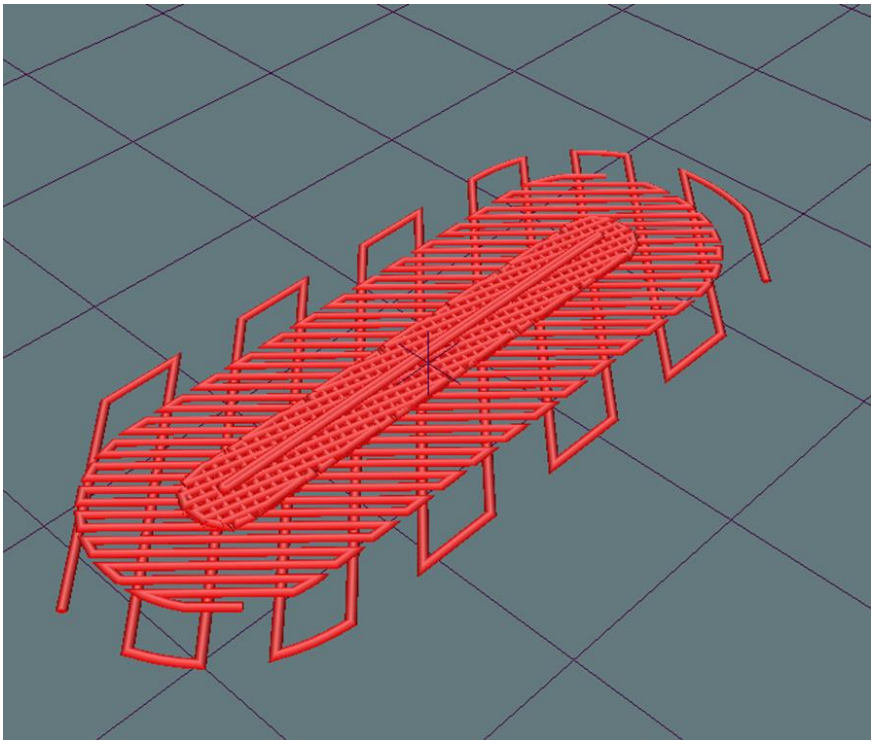

b)

Fig. 3.7. *(a) specimen printed with the SSI software; (b) design of the specimen reported in figure (a).*

The printed specimen is shown in Figure 3.7a; the quality is good, the line is straight, and the two filaments have a good bond. The Gcode indicates a different temperature for the nozzle while the raft is printed. In fact, this extra extruded material is printed at a temperature of 210 °C, while the main body is printed at a temperature of 200 °C. This can be explained since the raft has to bond perfectly with the carbon tray to oppose the lateral forces that the nozzle transmits during the printing process. Another observation was made regardless of the printing mode: the standard setting of the SSI software generates the Gcode in compliance with the absolute extrusion mode described in the previous chapter. Figure 3.8 shows an increase in the values written beside the letter E (that represent the volume of material extruded).

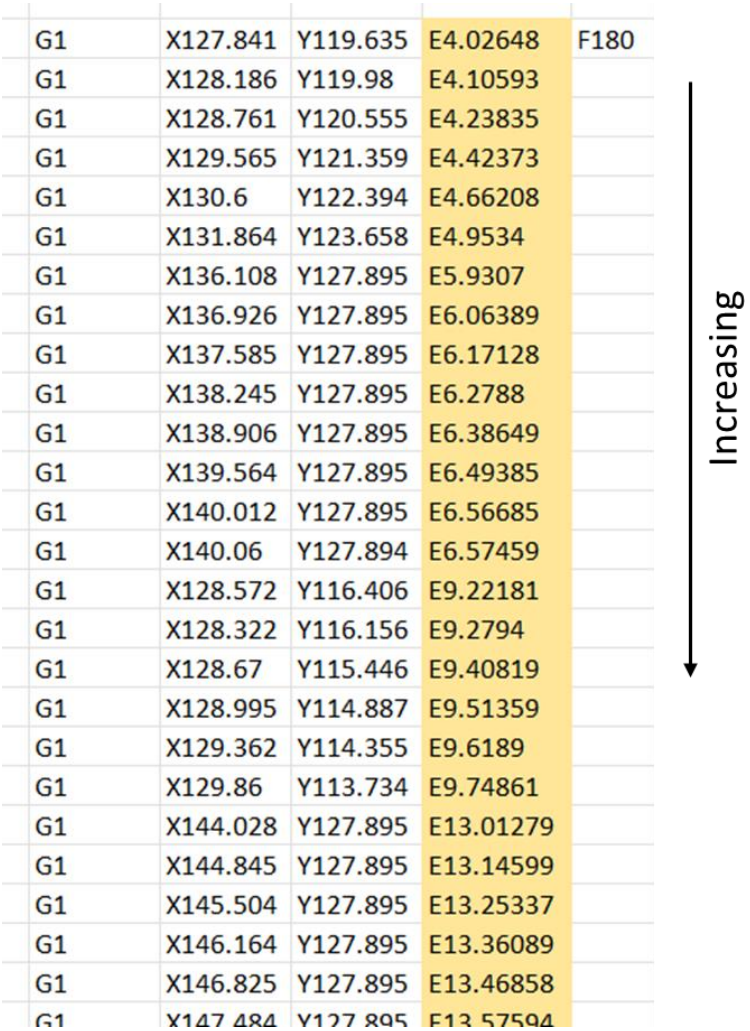

G1	X127.841	Y119.635	E4.02648	F180
G1	X128.186	Y119.98	E4.10593	
G1	X128.761	Y120.555	E4.23835	
G1	X129.565	Y121.359	E4.42373	
G1	X130.6	Y122.394	E4.66208	
G1	X131.864	Y123.658	E4.9534	
G1	X136.108	Y127.895	E5.9307	
G1	X136.926	Y127.895	E6.06389	
G1	X137.585	Y127.895	E6.17128	
G1	X138.245	Y127.895	E6.2788	
G1	X138.906	Y127.895	E6.38649	
G1	X139.564	Y127.895	E6.49385	
G1	X140.012	Y127.895	E6.56685	
G1	X140.06	Y127.894	E6.57459	
G1	X128.572	Y116.406	E9.22181	
G1	X128.322	Y116.156	E9.2794	
G1	X128.67	Y115.446	E9.40819	
G1	X128.995	Y114.887	E9.51359	
G1	X129.362	Y114.355	E9.6189	
G1	X129.86	Y113.734	E9.74861	
G1	X144.028	Y127.895	E13.01279	
G1	X144.845	Y127.895	E13.14599	
G1	X145.504	Y127.895	E13.25337	
G1	X146.164	Y127.895	E13.36089	
G1	X146.825	Y127.895	E13.46858	
G1	X147.484	Y127.895	E13.57594	

Fig. 3.8. *main body of the SSI Gcode for the sample shown in Figure 3.7.*

Second stage: first interaction with Fullcontrol software

The stage of starting the printing process was performed using Fullcontrol, taking into account the knowledge and structure introduced in the previous paragraphs. All the specimens have a unidirectional pattern, and they are printed directly on the carbon tray; the raft is not needed. Figure 3.9 shows a section of the main page in the Fullcontrol software. Each line is related to a string in the Gcode.

1	Line	Cartesian	155	105	0	R24.5	R0	R0	Print	0,3	0,15
2	Line	Cartesian	R0	R0	R0	R0	R-0.3	R0	Print	0,3	0,15
3	Line	Cartesian	R0	R0	R0	R-25,4	R0	R0	Print	0,3	0,15
4	Line	Cartesian	R0	R0	R0	R0	R-0,3	R0	Print	0,3	0,15
5	Cartesian repeat	1-4	0	-0,6	0	10					

Fig. 3.9. *section of the main sheet of Fullcontrol software showing the line that give the instruction to the machine.*

The user introduces the start and end coordinates and defines if the nozzle has to extrude material (print) or only travel between these two points (travel). In the same line, the dimensions of the filament are required to calculate the extrusion volume that will be written in the Gcode. The sketch shown in Figure 3.10 links each line written in the Fullcontrol software with the printing object. As it has been shown, some elements need to be repeated. Therefore, a new line named Cartesian repeat is introduced. The user must identify the commands that need to be repeated, the offset required (for example, the first four lines have a width [W] of 0.6 mm, so the user should use this dimension as offset), and lastly, the number of repetitions needed. The sample will have a final expression described by the following :

$$W = \left[(0.3 + 0.3) * 10 \right] + 0.3 = 6.3mm \tag{0.12}$$

This value was compared to the actual width of the printed sample.

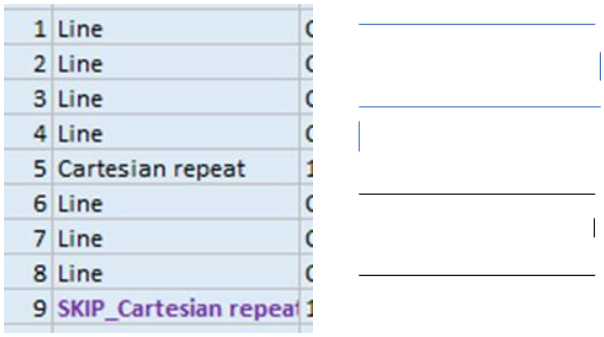

Fig. 3.10. *sketch of the instruction that each line gives to the machine through the Gcode.*

On the main page of Fullcontrol, some parameters can be changed based on the printing settings. Figure 3.11 shows the table where all these parameters are listed:

- Zoffset: define the offset between the bed and nozzle during the printing process,
- FirstLayerExtrusionMultiplier: this value will be multiplied by the extrusion value written after the letter E in the Gcode,

- FirstLayerNozzleSpeedMultiplier: as for the previous parameter this value will be multiplied by the nozzle speed written next to the letter F in the Gcode,
- NozzleFeedratePrintng: define the velocity of the nozzle during the extrusion process,
- NozzleFeedrateTravellig: define the velocity of the nozzle during movement between two coordinates,
- ExtrusionUnits: this parament is based on the printing setting.

Zoffset	0.3	mm
FirstLayerExtrusionMultiplier	1	no units
FirstLayerNozzleSpeedMultiplier	1	no units
ToolChange ID	Default	
Start tool (after StartGCODE)	0	
BedTemp	60	C
NozzleFeedratePrinting	1500	mm/min
NozzleFeedrateTravelling	2000	mm/min
NozzleTemp	210	C
FeedstockFilamentDiameter	2.85	mm
ExtrusionUnits	mm3	mm OR mm3
StartGCODE ID	A4V4	
EndGCODE ID	A4V4	
Start X (after StartGCODE)	20	mm
Start Y (after StartGCODE)	10	mm
Start Z (after StartGCODE)	0.3	mm
FanSpeed	0	
AutoTravelRetraction?	no	yes/no
- Threshold distance	1	mm
- Retraction (E-value)	5	mm OR mm3
- Retraction speed (F-value)	2500	mm/min
- Unretraction (E-value)	-5	mm OR mm3
- Unretraction speed (F-value)	2500	mm/min
- Z-hop	0.2	mm
- Z-hop speed (F-value)	7500	mm/min

Fig. 3.11. *table located in the main sheet of the Fullcontrol software listing all the parameters that can be changed by the user to match the machine setting.*

The setting used for the sample printed in this phase are summarized in the Table 3.2.

Table 3.2. Summary *of the printing setting adopted for the printed samples.*

Printing attempt	Parameters modify	change
1	ExtrusionUnits	mm
2	ExtrusionUnits	mm^3
3	ExtrusionUnits	mm^3
4	*FirstLayerExtrusionMultiplier*	*4*

The results are shown in Figure 3.12. As it can be seen, the first sample shows an over-extrusion rate of the material, and the printing quality does not reach the standards required for the membrane. The second attempt was successful, although an error in the Gcode was observed. Therefore, this printing test was not taken into account. The last attempt shows an improvement in the final quality, but it does not reach the standards. Moreover, the initial filaments are thin, while the last filament gets bigger. When comparing the width obtained from the equation (1.12) with the measured width, there is a slight difference, confirming that some filaments were not extruded.

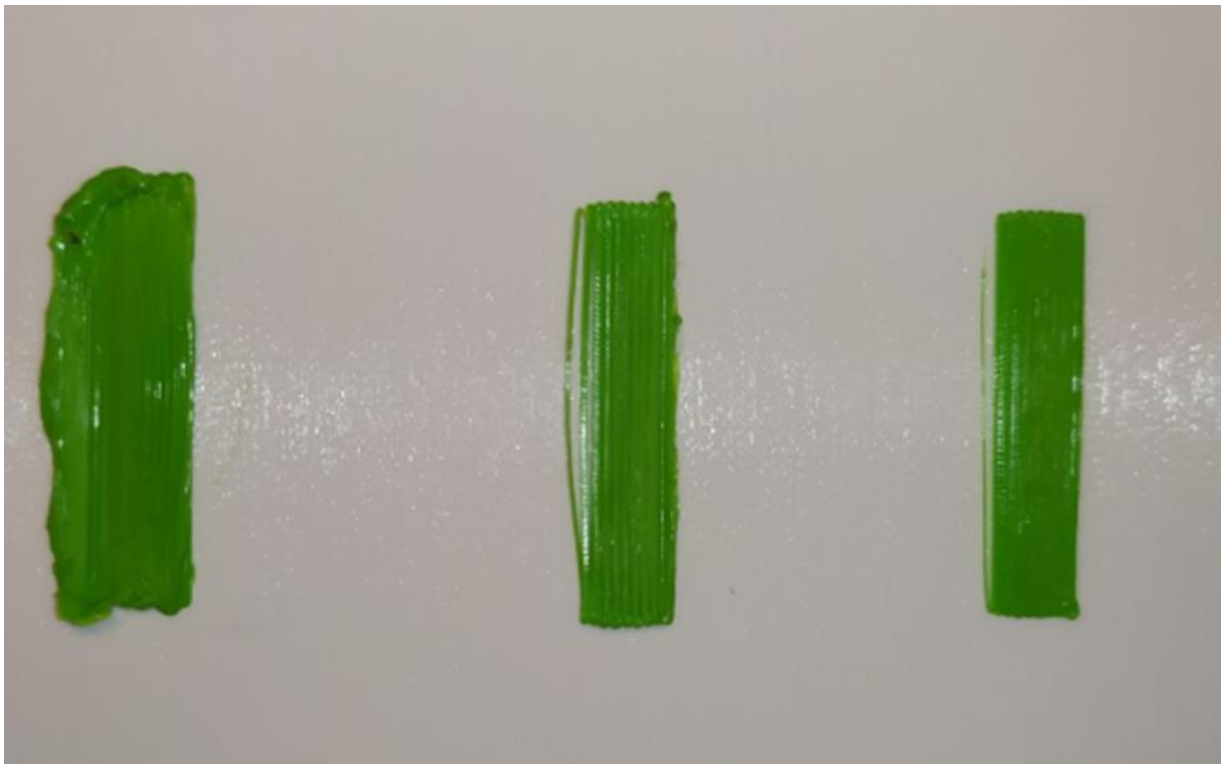

Fig. 3.12. *at the left the sample 1, at the center the sample 2, and last at the right the sample 3.*

The results obtained from the fourth specimen were similar to the previous attempt. A slight difference was observed regarding the extruded filaments. In fact, only half of the first filament was correctly extruded.

The outcome of this second phase shows that the FirstLayerExtrusionMultiplier can influence the quality of the filaments. Moreover, the offset of the filament can be enlarged to avoid an overlapping of the filaments that causes an undesired increase in the filament height.

Third stage: refinement of the *knowledge acquired*

Based on the experience gathered with the previous printing attempts, this stage was focused on refining the knowledge to have better confidence with the parameters and settings of both the A4V4 machine and Gcode software. The sample used in this phase is wider and has two layers; the infill pattern is unidirectional, and the infill density is 100%. Figure 3.13 shows the design of the sample; to avoid problems with the initial extrusion, two

additional filaments were introduced at the beginning (the slope filament in Figure 3.13) and at the end of the printing process.

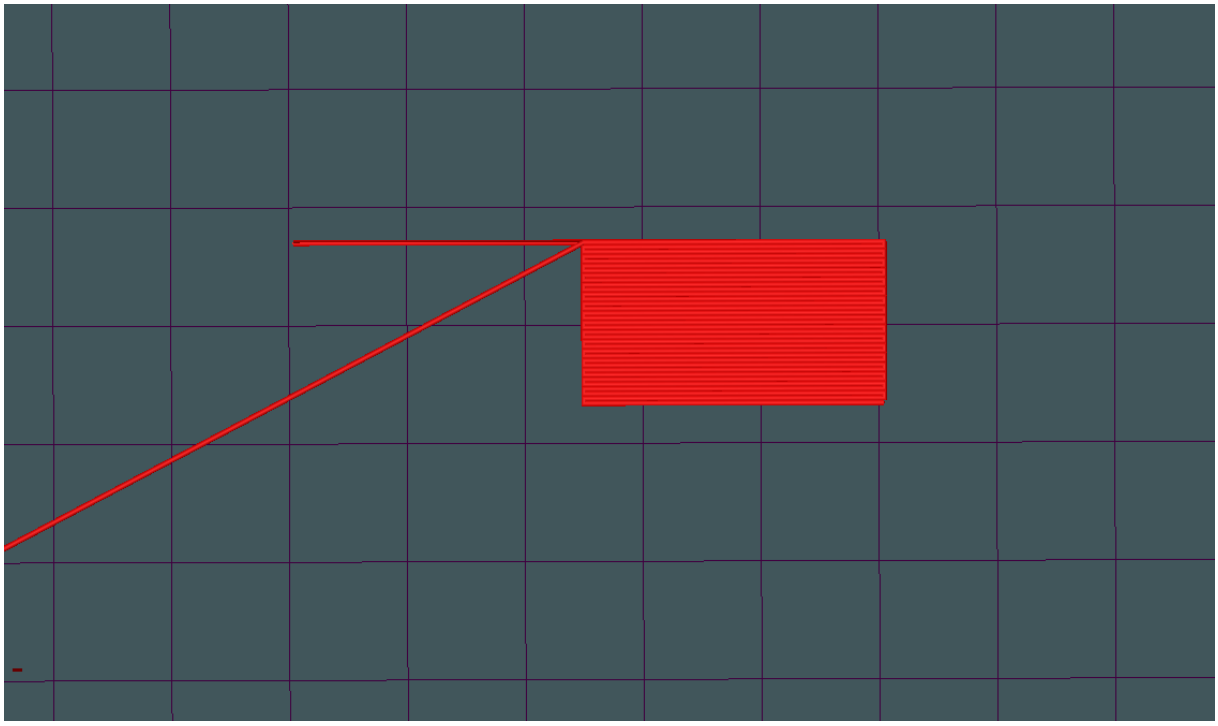

Fig. 3.13. *design of the sample printed during the third stage.*

Figure 3.14 shows a section of the main sheet in the Fullcontrol software. The line 1 gives the printer instructions to print the additional filament at the beginning of the printing process; the lines 2 to 5 describe the structure shown in Figure 3.14. In this case, the gap between the two lines is wider than the one adopted for the previous printing tests. Lines 6 and 7 complete the construction of the first layer, while line 8 moves the bed along the z axis to position the nozzle at the right height. From lines 9 to 13, the second layer is complete. Line 14 gives instructions to the machine to print an added length of the last filament.

1	Line	Cartesian	50	50	0	155	105	R0	Print	0,2	0,15
2	Line	Cartesian	R0	R0	R0	R25.4	R0	R0	Print	0,2	0,15
3	Line	Cartesian	R0	R0	R0	R0	R-0.4	R0	Print	0,2	0,15
4	Line	Cartesian	R0	R0	R0	R-25.4	R0	R0	Print	0,2	0,15
5	Line	Cartesian	R0	R0	R0	R0	R-0.4	R0	Print	0,2	0,15
6	Cartesian repeat	2-5	0	-0,8	0	16					
7	Line	Cartesian	R0	R0	R0	R+25.4	R0	R0	Print	0,2	0,15
8	Line	Cartesian	R0	R0	R0	R0	R0	R0.15	Travel	0,2	0,15
9	Line	Cartesian	R0	R0	R0	R-25.4	R0	R0	Print	0,2	0,15
10	Line	Cartesian	R0	R0	R0	R0	R0.4	R0	Print	0,2	0,15
11	Line	Cartesian	R0	R0	R0	R+25.4	R0	R0	Print	0,3	0,15
12	Line	Cartesian	R0	R0	R0	R0	R0.4	R0	Print	0,2	0,15
13	Cartesian repeat	9-12	0	0,8	0	16					
14	Line	Cartesian	R0	R0	R0	R-50	R0	R0	Print	0,2	0,15

Fig. 3.14. *section of the main sheet of Fullcontrol software showing the lines that give the instruction to the machine.*

The printed sample for the first attempt has a filament width of 0.3 mm and a height of 0.15 mm; the FirstLayerEstrusionMultiplier is set to 0.25, while the NozzleFeedratePrinting is equal to 500. The nozzle temperature is maintained at 200°C. The printed specimen shown in Figure 3.15 has a good quality; the spacing between layers prevented the overlapping of the filaments. The speed of printing is adequate; the first layer has good bonging with the carbon tray, and it does not get dragged by the nozzle. The speed of printing the second layer can be increased to reduce the printing time. The added filaments both at the beginning and end of the printing process led to better extrusion quality since the issue related to extrusion happened in this expendable section.

With the second attempt, the variation introduced concerned the printing velocity for the second layer, which increased from 500 to 1500. This variation was introduced in line 10. The printing was successful. The sample whose printing process is shown in Figure 3.15 exhibits excellent quality in the first layer; there are no overlapping filaments that are detectable with the naked eye without affecting the transversal bonding. All the filaments are printed, and the bonding with the carbon tray is good.

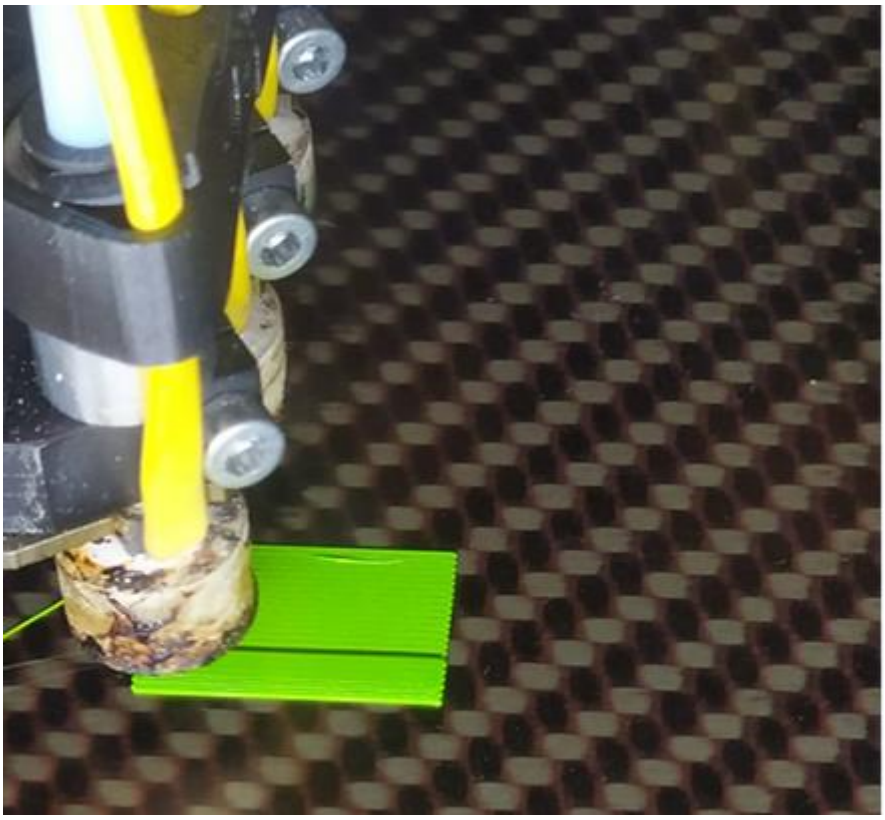

Fig. 3.15. *printing in progress for the specimen design by Fulcontrol. The machine has finished printing the first layer.*

In the following Figures 3.16 and 3.17 the settings used in this stage of the analysis are summarized:

Zoffset	0,2	mm
FirstLayerExtrusionMultiplier	0,25	no units
FirstLayerNozzleSpeedMultiplier	1	no units
ToolChange ID	Default	
Start tool (after StartGCODE)	0	
BedTemp	60	C
NozzleFeedratePrinting	500	mm/min
NozzleFeedrateTravelling	2000	mm/min
NozzleTemp	200	C
FeedstockFilamentDiameter	2,85	mm
ExtrusionUnits	mm3	mm OR mm3
StartGCODE ID	A4V4	
EndGCODE ID	A4V4	

Start X (after StartGCODE)	20	mm
Start Y (after StartGCODE)	10	mm
Start Z (after StartGCODE)	0,3	mm
FanSpeed	0	
AutoTravelRetraction?	no	yes/no
- Threshold distance	1	mm
- Retraction (E-value)	5	mm OR mm3
- Retraction speed (F-value)	2500	mm/min
- Unretraction (E-value)	-5	mm OR mm3
- Unretraction speed (F-value)	2500	mm/min
- Z-hop	0,2	mm
- Z-hop speed (F-value)	7500	mm/min

Fig. 3.16. *settings for the first sample attempt.*

Zoffset	0,2	mm
FirstLayerExtrusionMultiplier	0,25	no units
FirstLayerNozzleSpeedMultiplier	1	no units
ToolChange ID	Default	
Start tool (after StartGCODE)	0	
BedTemp	60	C
NozzleFeedratePrinting	500-1500	mm/min
NozzleFeedrateTravelling	2000	mm/min
NozzleTemp	200	C
FeedstockFilamentDiameter	2,85	mm
ExtrusionUnits	mm3	mm OR mm3
StartGCODE ID	A4V4	
EndGCODE ID	A4V4	
Start X (after StartGCODE)	20	mm
Start Y (after StartGCODE)	10	mm
Start Z (after StartGCODE)	0,3	mm
FanSpeed	0	
AutoTravelRetraction?	no	yes/no
- Threshold distance	1	mm
- Retraction (E-value)	5	mm OR mm3
- Retraction speed (F-value)	2500	mm/min
- Unretraction (E-value)	-5	mm OR mm3
- Unretraction speed (F-value)	2500	mm/min

- Z-hop	0,2	mm
- Z-hop speed (F-value)	7500	mm/min

Fig. 3.17. *setting for the second sample attempt.*

3.2 Compressive tests outcome

The forces acting on the PLA specimens during the compressive test were parallel to the axis A. Figure 3.18 shows the samples after the compression test is performed. As it can be observed, a similar deformation happened for all five PLA specimens (Figure 3.19); these distortions developed mainly once the yield stress was reached.

Fig. 3.18. *on the left the PLA specimen prior the compressive test and on the right the PLA specimen after the compressive test was performed.*

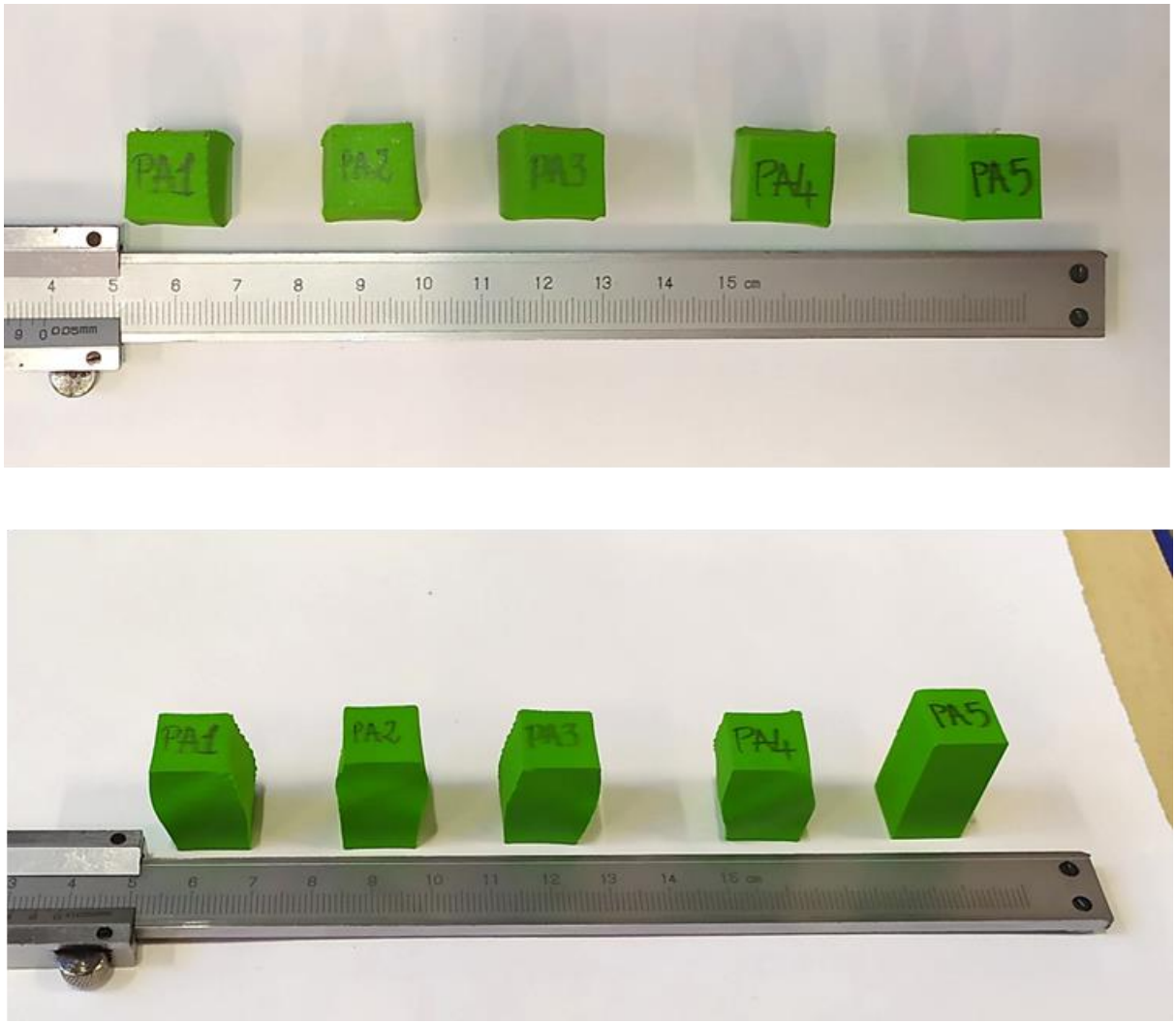

Fig. 3.19. *deformation of the specimens compared before and after the compression test were performed*.

The similarity between the behaviour of the specimens during the compression test is confirmed with the stress-strain curves shown in Figure 3.20. The first four specimens produced more comparable results for compressive strength, while the fifth specimen had the lowest compressive strength and modulus (31.96 MPa and 1.62 GPa). This behaviour is attributable to a malfunction of the printing machine due to the failure of the cooling system. Therefore, the fifth specimen has not been considered further in the evaluation of the average compressive strength and modulus.

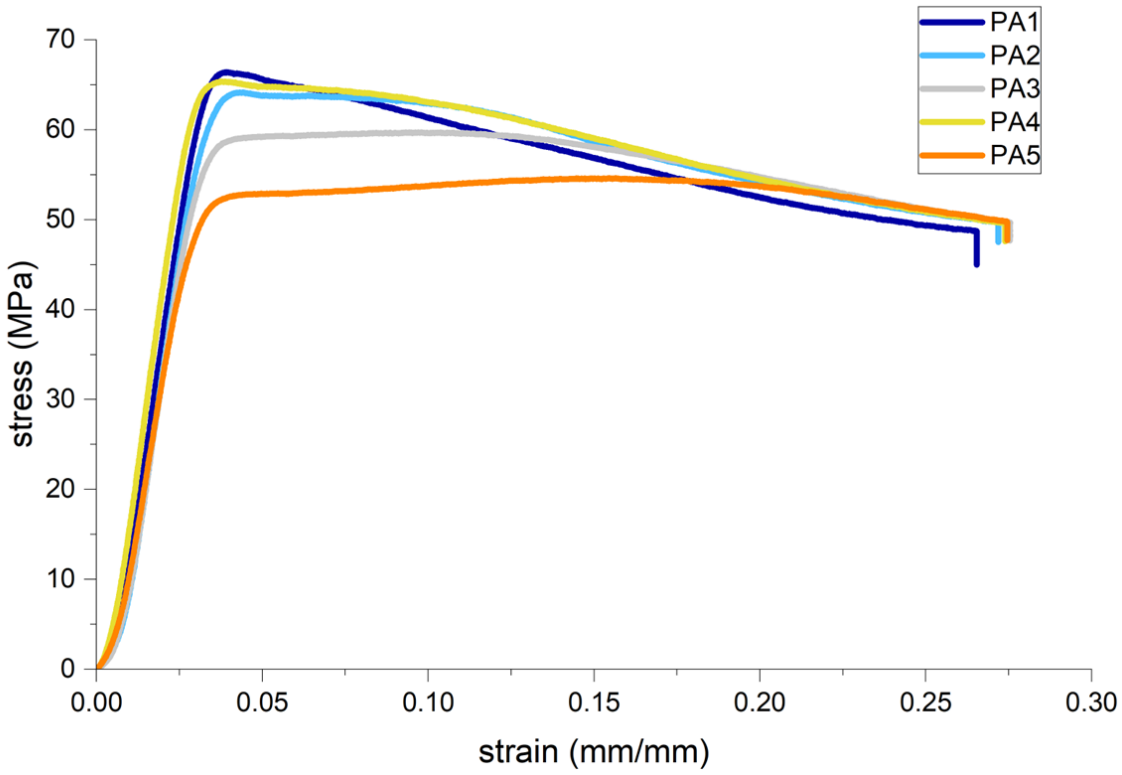

Fig. 3.20. *true stress-strain curves for the five specimens*.

The curves initially exhibit a nearly linear response caused by the adjustment of the compressive disk at the initial stage of the test. After the curves are linear till the yield stress is reached. The averages of the compressive strength and young modulus calculated from the true stress-strain curves are listed in Table 3.3.

Table 3.3. *Average of the Compressive strength and the Young's Modulus for the specimens.*

Specimen	Compressive strength [MPa]	Young's Modulus [GPa]
PA1	66.41	2.36
PA2	64.16	1.84
PA3	59.71	2.33
PA4	65.37	2.57
PA5*	31.96*	1.62*
Average	**63.91 ± 2.95**	**2.28 ± 0.31**

* These values are not considered to evaluate the average compressive strength and Young's modulus

The compressive mechanical properties were not affected by the printing orientation when comparing the outcomes with similar works in literature (Vukasovic et al. [27]; Prajapati et al. [30]; Ionut [31]) This is the case outlined by Vukasovic et al. [27], who performed compressive tests on specimens with different printing angles, showing that there isn't important dissimilarity between the results obtained for PLA specimens.

3.3 Analytical method outcome

Using the equation (1.5) introduced for the analytical approach to estimate the wavelength of the wrinkling instabilities, it is possible to relate the mechanical properties obtained from the compressive test with λc. Table 3.4 shows the wavelength determined for both models analysed, i.e., the first model with 1 mm film thickness and the second model with 0.2 mm film thickness.

Table 3.4. *Critical wavelength evaluated using equation (1.5).*

Model	Film thickness [mm]	Approach adopted to estimate λc	λc [mm]
1	1	equation (1.5)	1.84
2	0.2	equation (1.5)	3.68

The wavelength value was later confronted using the mechanical properties evaluated by other works that performed compressive tests on PLA (Vukasovic et al. [23]; Prajapati et al. [26]; Ionut [27]). Table 3.5 summarises the results obtained using the mechanical properties of the literature to evaluate the critical wavelength for both model 1 and model 2.

Table 3.4. *Critical wavelength evaluated using equation (1.5) and the mechanical properties from literature.*

Model	Film thickness [mm]	Approach adopted to estimate λc	λc [mm]
1	Vukasovic et al.	equation (1.5)	16.7
	Prajapati et al.		17.3
	Ionut		18.2
2	Vukasovic et al.	equation (1.5)	3.34
	Prajapati et al.		2.70
	Ionut		3.63

A further step was made in evaluating the critical force acting on the membrane once the wrinkling which wavelength is λc develops (Table 3.6). The depth of the model is assumed to be equal to one.

Table 3.6. *Critical force evaluated using equation (1.4).*

Model	Film thickness [mm]	Approach adopted to estimate F_c	F_c /depth [N/m]
1	1	equation (1.4)	9.08
2	0.2	equation (1.4)	1.72

3.4 Numerical simulation

The numerical simulation performed was carried out on the same model used for the analytical approach, assuming a plane stress condition. The analyses were computed with the Young's module obtained from the experimental tests for PLA, while for the TPU, the Young's module was considered equal to 30 MPa. The Poisson ratio adopted for both PLA and TPU materials was equal to 0.45. Linear analysis conducted on both models 1 and 2 exhibits a barrel deformation of the membrane (Figure 3.21).

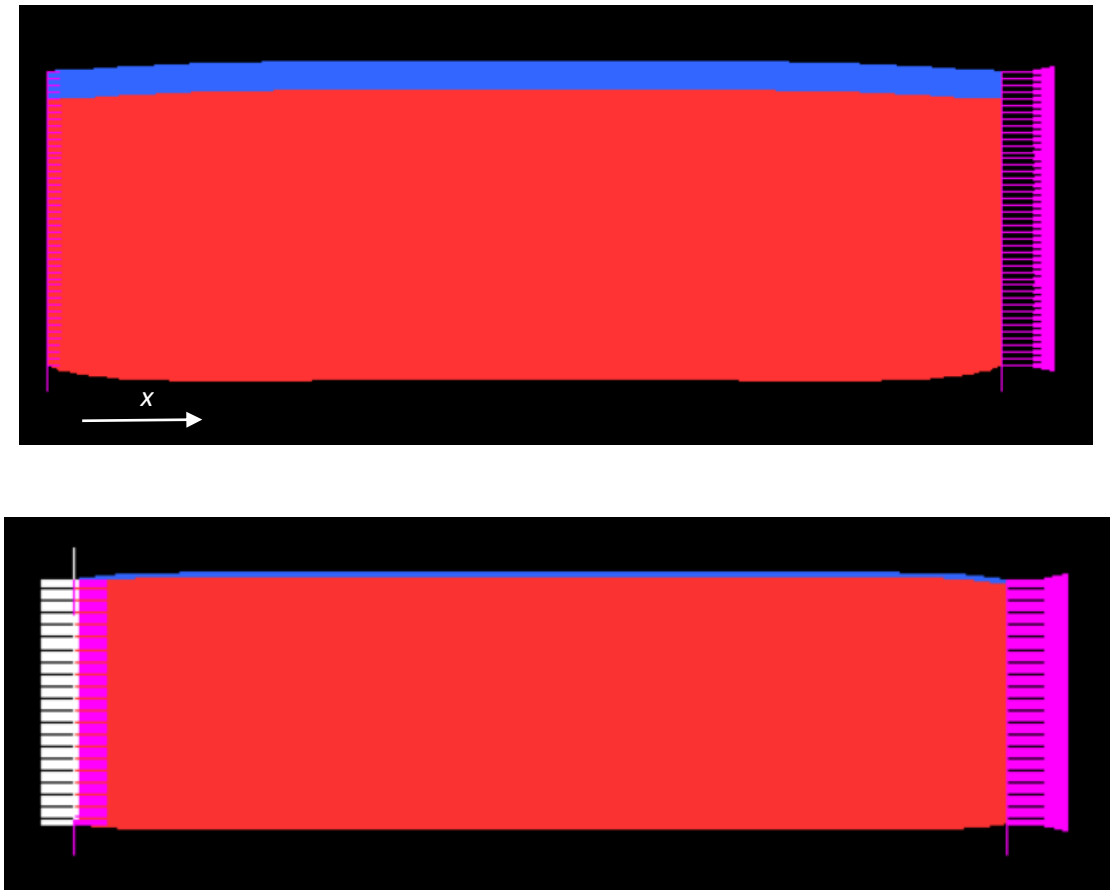

Fig. 3.21. *deformation observed with the linear analysis, on the top is shown the model 1 on the bottom is shown the model 2.*

Therefore, buckling analysis was performed to observe the instabilities in the thin layer of the membrane. The instability highlighted by this analysis is consistent with the theoretical knowledge introduced in Chapter 2 (Figure 3.22). In fact, it can be observed the

formation of wrinkles on the PLA thin layer. The critical wavelengths that were observed are equal to 2 mm for the model 1, while for the model 2, they are equal to 3.66 mm.

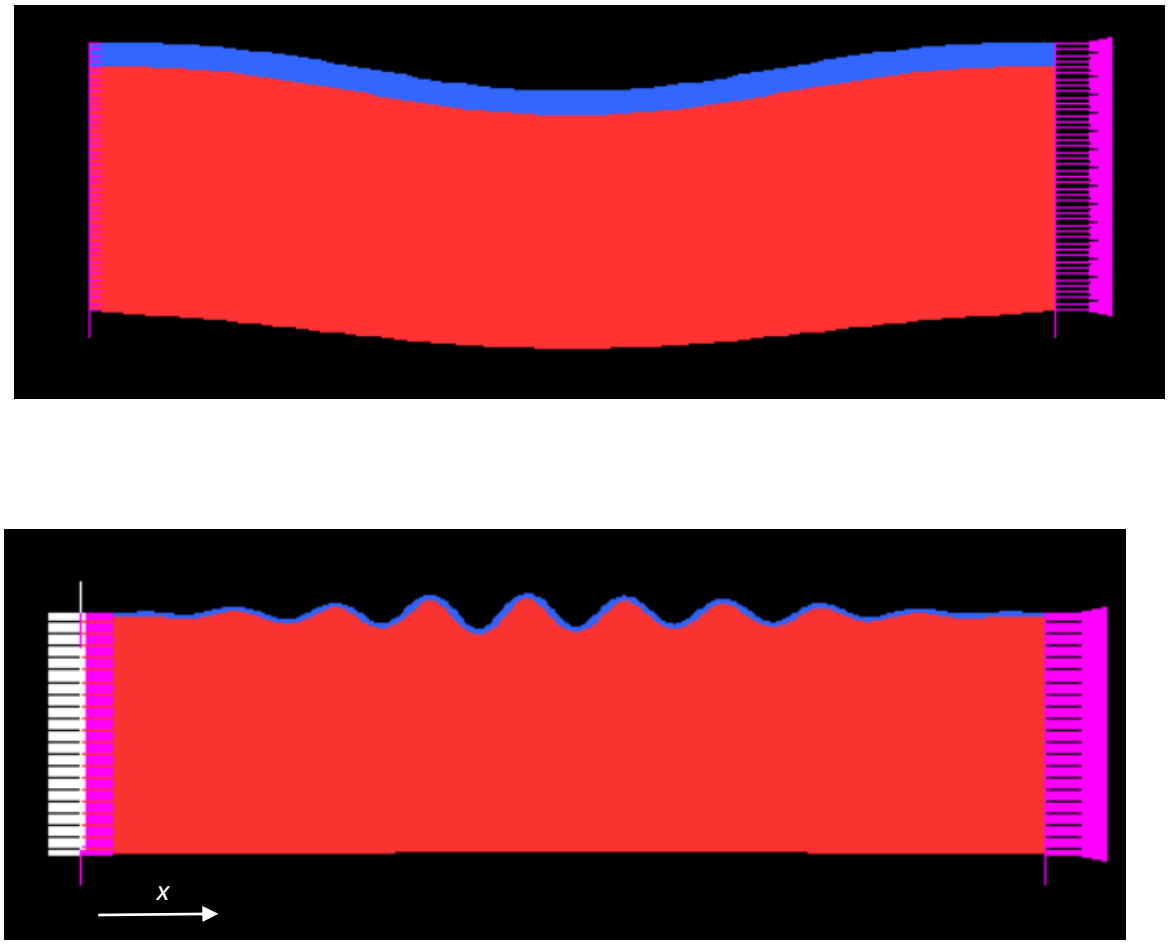

Fig. 3.22. *wrinkle phenomenon based on the result of the buckling analysis, on the top is shown the model 1, on the bottom is shown the model 2.*

Later, nonlinear analysis was conducted on the second model. To trigger the formation of wrinkles during the nonlinear analysis, an imperfection was introduced for the film layer. The entity of the imperfection was like the results obtained from the buckling analysis reduced so that the maximum displacement was less than or equal to the thickness of the film. The solution, shown in Figure 3.23, underlines the non-linearity of the wrinkle's formation on the film layer, and the wavelength is similar to the one evaluated with the bucking analysis.

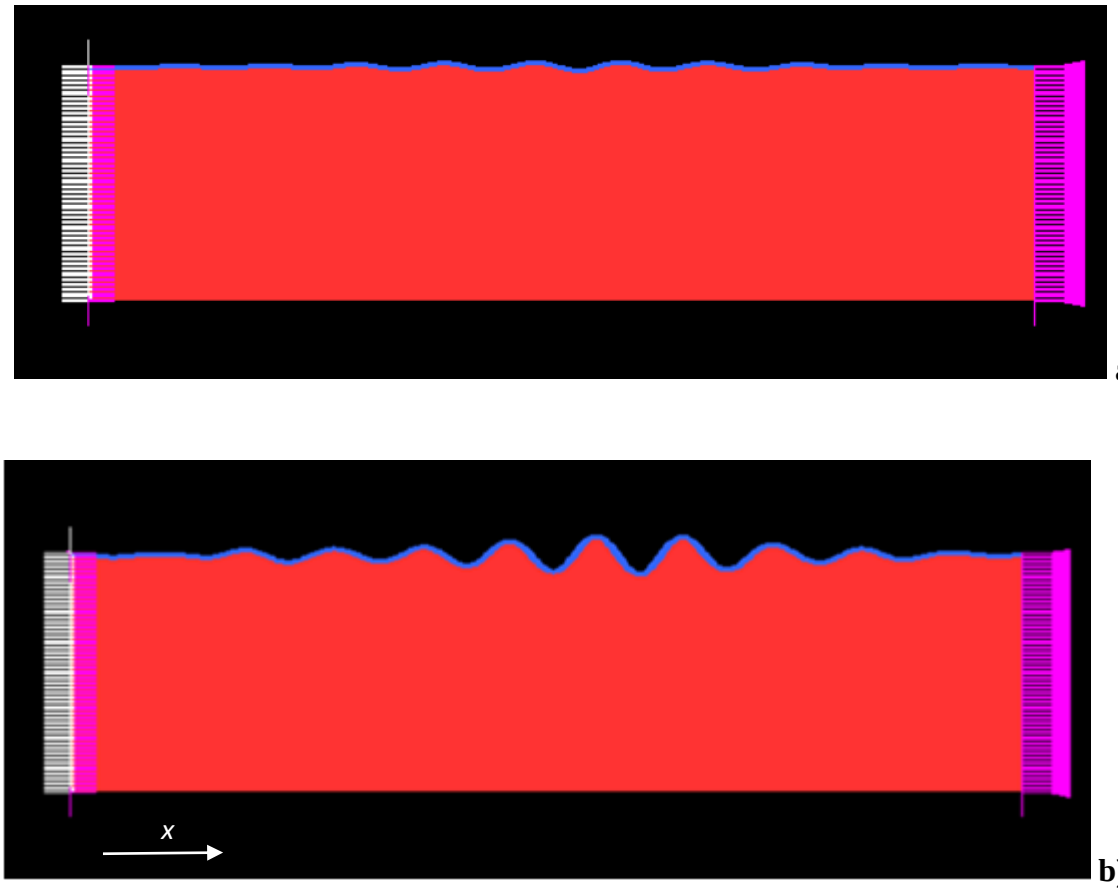

Fig. 3.23. *(a) imperfection introduced in the analysis; (b) result of the nonlinear analysis*.

4 DISCUSSION

The thesis has provided insight into understanding the wrinkling phenomenon in soft membranes that can be used to mimic leather and reduce the environmental footprint of this huge industry that is struggling to meet the constant, increasing demand for new goods [17]. The results of the study are commented on and elaborated on in this chapter, which also discusses the limitations and potential of additive manufacturing as well as how to interpret the results of analytical and numerical analysis.

(i) The specimen design for the compressive test and the soft membrane to mimic the tanned hides produced by a 3D printer using FDM technology were the main topics of the analysis's first section. Several Gcode structures were analysed by investigating the influence of the principal parameters involved in the design process to obtain the best results. Analysing the printing outcome for the sample with a unidirectional pattern made of PLA, the results meet the desired quality, as the adherence and sharpness of the filaments exhibit reliable properties. Moreover, the printing process was fast, and the waste was limited to the extra filaments introduced to avoid extrusion flaws. Although the construction of the Gcode employed a lot of time, the outcome can be seen as an investment of time since the Gcode does not necessitate modification to print the same object. In summary, the FDM printing allows us to obtain specimens of good quality while the customised Gcode improves the design process. Further experimentation is needed to establish the Gcode setting to print PLA and TPU as layers of a soft membrane. In fact, the two materials have to develop a good bond in order to withstand the compressive forces related to the formation of wrinkles. Avenues for future studies include printing:

- TPU sample with unidirectional pattern,
- PLA + TPU sample where the first material act as a raft for the second,

(ii) In order to define the Young's module to be included in the analytical and numerical simulation for the critical wavelength evaluation, a second experimental analysis was carried out to look into the mechanical properties under compression for a 3D printed specimen. The tests were carried out in compliance with the ASTM D695 standards. The Young's modulus and compressive strength evaluated via the compressive test are similar to the mechanical properties proposed by previous research [23, 25, 27–31].. The mean compressive Young's module value is 2.28 ± 0.31 GPa, while the mean compressive strength exhibits a value of 63.91 ± 2.95 MPa. The results obtained when compared with the research already conducted can give an overview of the mechanical properties of printed PLA. This work's novel contribution relates to the compressive characteristics of a specimen with a -/+ 45° infill pattern. Future research should focus on analysing the mechanical properties of specimens printed with a uniaxial filament infill pattern.

(iii) The purpose of this work was to compare the numerical simulation with the analytical method suggested by the research reviewed [10–12] to estimate the critical wavelength λc that appears on a compressed bilayer soft membrane. The analysis involved two bilayer system models; the first model's film thickness is 1 mm, while the second model's film thickness is 0.2 mm. The compressive test yielded the mechanical characteristics specific to PLA, whereas a literature review was done for TPU. λc was estimated using equation (1.5) and compared with the results obtained using the mechanical properties from the papers reviewed [27, 30-31]. Numerical simulation was used to conduct linear, buckling, and nonlinear analysis, and the outcomes were compared to those of the analytical approach. The results that can be drawn from this work are the following: The critical wavelength estimated with the analytical approach is consistent with the results obtained using the mechanical properties of the literature; the main dissimilarity is related to the infill pattern of the printed specimens used for the compressive tests. The relevant results acquired with numerical simulation outline a similarity with the value of the analytical approach. Therefore, we can state that the analytical approach applied to a membrane made of PLA and TPU is a valid tool to

estimate the wrinkling critical wavelength. In addition, knowing the wavelength of this surface instability, the mechanical properties of the other material, and lastly, the thickness of the film, can be used to estimate the mechanical properties of one of the membrane materials using the analytical approach. For this reason, a more detailed experimental analysis of the soft membrane can be conducted in the future. This would make it possible to comprehend the restrictions that the analytical method may impose on the determination of the wrinkle's critical wavelength.

5 CONCLUSION

The aim of this work was to validate the analytical approach used to predict the formation of wrinkles within a film layer on a soft membrane resembling leather material. Despite the difficulties encountered with the printing process for the specimen made from TPU, additive manufacturing represents a valid solution that can be implemented in the leather industry to help make the manufacturing process more sustainable in the future (Buljan et al. [17]). Nowaday, the footwear industry was able to develop shoe completely made using additive manufacturing, this is the case of the brand Nike, that developed a running shoe using an FDM printer and TPU as main material for the upper part [20]. The design and printing process for the PLA specimens was fast and simple, and only a small quantity of recyclable waste was generated (i.e., the raft). Thus, FDM printing can contribute to a more sustainable means of production by minimising the amount of water and harmful chemicals employed in the leather industry while at the same time improving the working environment. Another important aspect regards the possibility of reducing the cruelty towards the animals engaged in the leather industry. The entire process was quick and smooth, and at the same time, the Gcode made it simple to produce the desired final object.

Both PLA and TPU are materials that can be combined to recreate a leather-like membrane. Moreover, PLA is biodegradable. A more detailed study should be carried out to investigate the bonding between these two materials. In fact, since the wrinkling instabilities occur once the critical force is reached, a debonding phenomenon could happen at that stage.

The results obtained by the numerical simulation validate the analytical approach equation (1.5). Moreover, the magnitude of the critical wavelength estimated for the soft membrane made of PLA and TPU is similar to that observed on tanned rawhide by Genzer and Groenewold [10].

References

[1] B. Li, Y. Cao, X. Feng, H. Gaoc, “Mechanics of morphological instabilities and surface wrinkling in soft materials: a review”, Soft Matter, 2012.

[2] Y. Cao, Y. Jiang, B. Li, X. Feng, “Biomechanical modelling of surface wrinkling of soft tissues with growth dependent mechanical properties”, Acta Mechanica Solida Sinica, 2012.

[3] G. Limbert, “Mathematical and computational modelling of skin biophysics: a review”, The Royal society Publishing, 2017.

[4] D. Bakiler, A. Javili, “Understanding the role of interfacial mechanics on the wrinkling behavior of compressible bilayer structures under large plane deformations”, Mathematics and Mechanics of Solids, 2022.

[5] J. Zhang, Y. Li, Y. Xing, “Theoretical and experimental investigations of transient thermo-mechanical analysis on flexible electronic devices”, Int J Mech Sci., 160: 192–199, 2019

[6] B. M. Haines, J. R. Barlow, “Review The anatomy of leather”, Materials science, 1974.

[7] D. Dillard, B. Mukherjee, P. Karnal, R. Batra, J. Frechette, “A review of Winkler’s foundation and its profound influence in adhesion and soft matter applications”, Soft Matter, 2018.

[8] A. Evans, E. Cheung, K. Nyberg, A. Rowat, “Wrinkling of milk skin is mediated by evaporation”, Soft Matter, 2017.

[9] Y. Cao, J. Hutchinson, “Wrinkling Phenomena in Neo-Hookean Film/Substrate Bilayers”, Journal of Applied Mechanics, 2012.

[10] J. Genzer, J. Groenewold, “Soft matter with hard skin: From skin wrinkles to templating and material characterization”, Advanced Drug Delivery Reviews, 2006.

[11] E. Cedra, L. Mahadevan, “Geometry and Physicas of Wrinkling. Physical Review Letter”, 2003.

[12] M. A. Biot, “Surface instability of rubber in compression”, Appl. Sci. Res., 1961.

[13] L. Mogos-Soldevila, G. Matzeu, G. Lo Presti, F.G. Omenetto, “Additively manufactured leather-like silk protein materials”, Material design, 2022.

[14] I.Kráľ, F. Schmėl, J. Buljan “The future for leather”, 2014 1

[15] Britannica, The Editors of Encyclopaedia. "tanning". Encyclopedia Britannica, 19 Feb. 2018, https://www.britannica.com/technology/tanning. 2

[16] https://www.carlfriedrik.com/int/magazine/vegetable-tanned-leather 3

[17] J. Buljan, I. Kràl’, “The framework for sustainable leather manufacture”, 2019.

[18] ASTM International, 2013. F2792-12a - Standard Terminology for Additive Manufacturing Technologies. Rapid Manufacturing Association 10–12.

[19] A. Jadhav, V. S. Jadhav, “A review on 3D printing: An additive manufacturing technology”, Material today: Proceedings, 2022.

[20] “Additive Manufacturing (3D printing) How can it be used by the footwear and leather goods sectors?”, World Footware Innovation Paper, 2022

[21] F. Calignano, V. Mercurio, “An overview of the impact of additive manufacturing on supply chain, reshoring, and sustainability”, Cleaner Logistics and Supply Chain, 2023.

[22] T. A. Nezwek, M. Varacallo, “Physiology, Connective Tissue”, StatPearls Publishin, 2022

[23] J. M. Mercado-Colmenero, M. A. Rubio-Paramio, M. D. La Rubia-Garcia, D. Lozano-Arjona, C. Martin-Donate, “A numerical and experimental study of the compression uniaxial properties of PLA manufactured with FDM technology based on product specifications”, The International Journal of Advanced Manufacturing Technology, 2019.

[24] Materials, E. I. (n.d.) “Standard test method for compressive properties of rigid plastics. ASTM D695” InsulatingStandards, Annual Book of ASTM

[25] P. Yadav, A. Sahai, R.S. Sharma, “Strength and Surface Characteristics of FDM-Based 3D Printed PLA Parts for Multiple Infill Design Patterns”, The Institution of Engineers (India), 2021.

[26] J.R. Barber, “Contact Mechanicas”, Solid Mechanics and its Applications, 2018.

[27] T. Vukasovic, J. F. Vivanco, D. Celentano, C. Garcìa-Herrera, “Characterization of mechanical response of thermoplastic parts fabricated with 3D printing”, The international Journal of Advanced Manufacturing Technology, 2019.

[28] Souissi S., Bennour W. Elloumi A., Mechanical properties of 3D printer parts: effect of ultraviolet PLA filaments ageing and water absorption, Sage journals (2022)

[29] Rodriguez-Panes A., Claver J., Camacho A.M., The influence of manufacturing parameters on the mechanical behaviour of PLA and ABS pieces manufactured by FDM: A comparative Analysis, Materials (2018)

[30] A. R. Prajapati, S. R. Rajpurohit, N. H. Patadiya, H. K. Dav, “Analysis of Compressive Strength of 3D Printed PLA Part, Advances in Manufacturing Processes” 2021.

[31] O. Ionut, “PLA 3D compressive Test”, 2021.

NTNU
Norwegian University of
Science and Technology

UNIVERSITÀ
DI PARMA